Hydrol. Earth Syst. Sci. Discuss., doi:10.5194/hess-2016-109, 2016
Manuscript under review for journal Hydrol. Earth Syst. Sci.
Published: 9 March 2016

Hydrology and Earth System Sciences Discussions

Exploring the interplay between state, structure and runoff behaviour of lower mesoscale catchments

Simon Paul Seibert[1], Conrad Jackisch[1], Uwe Ehret[1], Laurent Pfister[2], and Erwin Zehe[1]

[1]Karlsruhe Institute of Technology (KIT), Institute for Water and River Basin Management, Chair of Hydrology, Kaiserstrasse 12, 76131 Karlsruhe, Germany
[2]Luxembourg Institute of Science and Technology, Department Environmental Research and Innovation, Catchment and Eco-hydrology research group, 5 avenue des Hauts-Fourneaux, L-4362 Esch/Alzette, Luxembourg

Correspondence to: Simon P. Seibert (simon.seibert@kit.edu)

Abstract. The question of how catchments actually "function" has probably caused many sleepless nights as it is still an unsolved and challenging scientific question. Here, we approach this question from the similarity perspective. Instead of comparing single physiographic features of individual catchments we explore the interplay of state and structure on different runoff formation processes, aiming to infer information on the underlying "functional" behaviour. Therefore, we treat catchments as lumped terrestrial filters and relate a set of different structure and storage descriptors to selected response measures. The key issue here is that we employ dimensionless quantities exclusively by normalizing the variable of interest by its limiting terrestrial or forcing characteristic. Specifically we distinguish extensive/additive and intensive/non-additive attributes through normalizing storage volumes by maximum storage capacities and normalizing fluxes (e.g. discharge) by permeability estimators. Moreover, we propose the normalized temporal derivative of runoff as a suitable measure to detect intensity-triggered (high frequency) runoff production.

Our dimensionless signatures evidently detect functional similarity among different sites for baseflow production, storm runoff production and the seasonal water balance. Particularly in the latter case we show that normalized double and triple mass curves expose a typical shape with a regime shift that is clearly controlled by the onset and the end of the vegetation period which we can adequately characterize by a simple temperature index model. In line with this, temperature explained 70 % of the variability of the seasonal summer runoff coefficients in 22 catchments distributed along a strong physiographic and climatic gradient in the German part of the Danube basin. The proposed non-additive response measure detected signals of high frequency intensity controlled runoff generation processes in two alpine settings. The approach, in fact edge filtering, evidently works when using "low-pass" filtered hourly rainfall-runoff data of mesoscale catchments ranging from 12 to 170 km^2.

We conclude that vegetation exerts a first order control on summer stream flow generation when the onset and termination of summer are more significantly defined by temperature than simply by the actual Gregorian day. We also provide evidence that properties describing gradients (e.g. surface topography) and resistances (e.g. hydraulic conductivities) may be much more powerful in explaining runoff response behaviour when they are treated as groups compared to their individual use. Lastly, we show that storage estimators such as the proposed normalized versions of pre-event discharge and antecedent moisture can be valuable predictors for event runoff coefficients: For some of our test regions they explain up to 70 % of their variability.

1 Introduction

1.1 Hydrological similarity as a weak form of causality

How close must two catchments be with respect to state and structure such that they produce runoff in a similar way? Based on the findings of Dooge (1986) we establish our studies essentially on the expectation that hydrological systems are essentially deterministic. Hence, identical inputs of energy and rainfall will cause an identical runoff response, if two identical catchments are in the same state. This crude deterministic paradigm is, however, of low practical use, because neither the system state nor the structural setup are exhaustively observable. Hence, we can at best postulate that similarity of structure and state of a terrestrial system implies "similar" functioning (Wagener et al., 2007; He et al., 2011; Zehe et al., 2014). While such a weak form of causality may be easily defined in qualitative terms, its translation into useful similarity measures for structure, state and runoff response is far from being a straight forward exercise, particularly at the lower mesoscale.

1.2 Challenges in defining structural similarity at the lower mesoscale

Parts of the confusion stem from the inherent equifinality and non-uniqueness of most of our governing equations (Beven, 1989; Zehe et al., 2014). This is particularly true for runoff because an integrated mass flux leaving a catchment control volume is a non-unique product of a driving potential gradient and the control volume conductance (or its inverse resistance). This implies that systems that largely differ with respect to the topographical controls on the driving gradients and the pedo-geological controls on the integral conductance may produce runoff in a similar fashion (Binley and Beven, 2003; Wienhöfer and Zehe, 2014). Topographic controls and pedological controls on runoff generation must thus be interpreted as group, to be able to judge how they jointly control runoff behaviour. This requires metric data sets on topography as well as on soil water and aquifer characteristics. While the former is available as highly resolved digital elevation and landuse maps, the latter can in most cases at best be estimated using (very) coarse soil and geological maps in combination with pedo-transfer functions - not to mention the absence of data characterising preferential pathways. It is, hence, no surprise that many model-based similarity studies rely on categorical soil and landuse data and translate them into metric catchment descriptors by means of their areal share (e.g., Merz and Blöschl, 2003; Hundecha and Bárdossy, 2004; Carrillo et al., 2011; Sawicz et al., 2011; Ali et al., 2012; Kelleher et al., 2015). Notwithstanding that this approach is feasible when representing similar catchments by similar parameters in conceptual models, it is way too simple to be conclusive for similarity of runoff production in the real world.

1.3 Storage estimators and state estimators - how to normalize and how to achieve coherence?

Storage estimators such as antecedent precipitation (Heggen, 2001; Brocca et al., 2009), pre-event discharge (Refsgaard, 1997; Graeff et al., 2012) or dynamic storage (Sayama et al., 2011) have been shown to be helpful to characterise storage in the catchment control volume and the related runoff proneness across scales (Tetzlaff et al., 2011). This is particularly appropriate when subsurface storage capacity controls runoff production (Struthers and Sivapalan, 2007; Struthers et al., 2007a, b), which implies runoff to monotonically increase with storage and thus to be limited by additive quantities. Such quantities are rainfall depth and saturation deficit in the case of saturation excess (Dunne and Black, 1970), or rainfall depth and subsurface storage in the case of subsurface storm flow (Tromp-van Meerveld and McDonnell, 2006; Lehmann et al., 2006).

Additive storage measures can easily be derived from either the catchment water balance or observed rainfall and discharge volumes (McNamara et al., 2011) and equally easily be upscaled, as soil and aquifer water content are additive quantities. However, absolute storage is difficult to compare between different pedolological settings as these measures require a meaningful normalization in order to be related to runoff processes. Furthermore, dynamic storage (Sayama et al., 2011) depends on the starting point of integration. As catchment inter-comparison studies should compare coherent time series, this starting point needs to be carefully chosen to ensure that integration starts at the same relate storage state. When the catchments of interest are spread across a wide topographic and climatic range, the same Gregorian day might be a very inappropriate choice, as further elaborated in section 2.1.

Notwithstanding the importance of storage estimators, they do not provide a full characterization of the catchment state. The latter particularly requires information on where in the catchment the water is stored (Nippgen et al., 2015) and whether it is subject to strong, weak or no capillary and/ or osmotic forces. Unfortunately, soil water potentials, plant water potentials and piezometric heads are intensive state variables and thus non-additive. They can neither be determined as residuals of a balance equation nor can they easily be scaled up in an additive manner (Zehe et al., 2006; de Rooij, 2009, 2011). Hence, characterization of the full system state requires comprehensive, spatially highly resolved data sets on both soil moisture and soil water potentials (Zehe et al., 2013). As these are rarely available in mesoscale catchments, similarity and catchment inter-comparison studies are challenging to work with, giving a fairly incomplete characterisation of the system state. This is particularly unpleasant because it is the potential gradients which determine the "forces" driving water and energy fluxes (Kleidon, 2012; Zehe et al., 2014).

1.4 Dimensionless response measures for and beyond capacity controlled runoff formation

The striking success of similarity theory and scaling based on dimensionless quantities throughout a range of disciplines such as hydraulics (e.g. Reynolds, Froude, Péclet number), acoustics (e.g. Helmholtz number), chemistry (e.g. Dammköhler numbers) or micro meteorology (e.g. the Monin–Obukhov length) motivated past research for useful dimensionless quantities characterizing hydrological similarity (e.g., Saghafian et al., 1995; Reggiani et al., 2000; Woods, 2003; Berne et al., 2005; Struthers et al., 2007b; Woods, 2009; Schaefli et al., 2011). The Budyko curve (Budyko, 1961) is probably the most generally accepted dimensionless analysis technique in hydrology to assess similarity in the steady state water balance by plotting the evaporative fraction against a dryness index. In line with these studies we hypothesize that dimensionless state-response diagrams are suitable candidates for similarity assessment for catchment inter-comparison. Proper normalization of state and response measures means to normalize using those climate and terrestrial system properties which limit runoff production. The rationale is that one can expect these dimensionless plots to remain invariant, as long as the limiting factors remain unchanged.

Normalization in the case of capacity controlled runoff formation is straightforward as it is limited by additive quantities, essentially storage and rainfall volumes. We may hence treat catchments as lumped terrestrial filters (Black, 1997) and normalize event scale runoff by total precipitation amount, and relate this to storage estimators such as antecedent precipitation (Heggen, 2001; Blume et al., 2007; Graeff et al., 2012), dynamic storage (Sayama et al., 2011) or pre-event discharge (Graeff et al., 2009; Kirchner, 2009; Zehe et al., 2010). A feasible normalization of storage estimators should be based on the minimum and maximum subsurface storage volume/depth or, if this information is not available, on the storage depth in the root zone of the soil. Similarly, we may compare annual double mass curves of normalized accumulated rainfall and runoff fluxes to discriminate differences in the seasonal interplay of storage and release (Pfister et al., 2002; Hellebrand et al., 2008). Although all these measures and their normalization can in principle be determined as residuals of the water balance and from available maps, the devil lies in the details as further elaborated in section 2.1.

Detection and normalization of intensity controlled runoff production is, however, not that straight forward (Struthers and Sivapalan, 2007). Intensity controlled runoff generation is characterized by intensive, convective rainfall forcing and a fast, high frequency stream flow response, reflecting onset of rapid subsurface flows (Lehmann et al., 2006; Wienhöfer and Zehe, 2014) and/ or infiltration excess (Niehoff et al., 2002; Zehe et al., 2005). The latter is difficult to observe *in situ* during natural forcing conditions but its occurrence is well known from many artificial rainfall simulation experiments (e.g., Fiener et al., 2011, 2013). Intensity controlled runoff production occurs in a threshold like manner (Lehmann et al., 2006; Zehe and Blöschl, 2004; Struthers and Sivapalan, 2007; Zehe et al., 2007; Ruiz-Villanueva et al., 2012) and is neither controlled (and limited) by additive rainfall properties nor by current storage. Hortonian overland flow production is for instance controlled (and limited) by the relationship of non-additive rainfall intensity and soil infiltrability (Horton, 1939; Hohmann, 2014). The latter is a conglomerate of unsaturated hydraulic conductivity, and suction head as well as of the density, depth and capacity of apparent macropores (Beven and Germann, 2013). Again, none of these quantities is additive during up-scaling.

As intensity control implies i) the high frequencies to be dominant and ii) first order control of non-additive characteristics, any form of spatial and temporal data aggregation essentially implies to loose parts or even the complete signal due to low-pass filtering. There are promising options to assess highly resolved patterns of rainfall based on weather radar (e.g., Ehret et al., 2008; Kneis and Heistermann, 2009) or to estimate catchment scale patterns of biotic macropores (Palm et al., 2013; Van Schaik et al., 2014). However, discharge as our best observation of runoff formation inevitably represents a convolution of distributed runoff production and concentration, which inherently implies low-pass filtering.

A cardinal question is thus on the minimum requirements for detecting intensity controlled runoff generation. Related studies often operate at relatively small scales, relying on high frequency rainfall-runoff data in combination with breakthrough or flushing of either contaminants (Gassmann et al., 2013), artificial tracers (Wienhöfer et al., 2009), sediments (Martínez-Carreras et al., 2010) or even diatoms as *smart* tracers (Martínez-Carreras et al., 2015; Klaus et al., 2015). Most "operational" data sets however do not offer these sources of extra information and are at best available at an hourly resolution and for catchment sizes $\geq$ 40-50 km^2. The challenge to detect intensity controlled runoff production within inter-comparison studies seems at first sight similar to the challenge to repair a watch with a monkey wrench. One way forward might be to relate temporal changes in rainfall intensities to temporal changes in runoff - which means in fact to analyse the acceleration of input and output fluxes, as further elaborated in section 4.4.

1.5 Objectives and research questions

While being fully aware of all the listed challenges and shortcomings of operationally available data sets, we propose and test dimensionless measures to discriminate differences in runoff generation (storage and/ or intensity controlled) in lower mesoscale catchments. In particular, we pose three main questions:

- Question 1: How feasible is the use of dimensionless state and/or storage-response diagrams to detect differences in event scale flood production, baseflow generation and the seasonal water balance?

Hydrol. Earth Syst. Sci. Discuss., doi:10.5194/hess-2016-109, 2016
Manuscript under review for journal Hydrol. Earth Syst. Sci.
Published: 9 March 2016

Hydrology and Earth System Sciences Open Access Discussions

– Question 2: Can we detect intensity controlled runoff formation as essentially a high frequency process based on low frequency data?

– Question 3: Which structural, climatic and ecological catchment characteristics explain the differences between different catchments and among different years and which of them operate in groups?

Our study area is the Bavarian part of the Danube basin in Southern Germany, which we introduce in detail in section 3 together with the data and model we use. More specifically, we use an operational data set from the federal water resources management agency and standard categorial data on landscape characteristics in about 130 lower mesoscale catchments. Additionally, we apply a calibrated water budget model which covers all of the sub-basins to ensure a consistent estimation of evapotranspiration and storage estimators such as dynamic storage. Particular emphasis within our inter-comparison study is on the issues of i) proper normalization of storage estimators and fluxes, ii) assuring coherence and similar quality of associated time series and iii) on an assessment of the different storage estimators with respect to explanatory power and redundancy.

2 Conceptual framework and candidate diagnostics

In this section we propose a set of dimensionless "functional diagnostics", suitable for catchment inter-comparison studies across a wide range of end members. Hence, we exclusively rely on commonly available landscape properties and hydro-meteorological data.

2.1 Requirements of functional diagnostics

Useful diagnostics for runoff response and catchment state need to be sensitive to the limiting factors and allow for a normalization of the responses and state variables to i) separate meteorological from terrestrial controls and ii) to test our perception on underlying structural controls. We expect intensity controlled runoff production to occur in landscapes characterized by strong gradients, shallow and poorly developed soils, high abundances of either very coarse or fine/clay substrates, sparse surface coverage, and/or geologies which develop rift aquifers. Capacity controlled runoff generation is deemed to dominate in landscapes characterized by weak gradients, well drained and homogeneous textured soils (without remarkable clay or skeleton contents), and medium to high degrees of surface cover over parent materials that sustain pore aquifers. Also snow dominated areas are expected to exhibit capacity controlled behaviour. At the seasonal scale we additionally need to make sure of comparing coherent time series of similar data quality.

2.1.1 Normalization of states and response measures

In our study we compare three storage estimates: a rescaled version of dynamic storage, accumulated antecedent precipitation and pre-event discharge (see details in section 2.2). All three surrogates

Hydrol. Earth Syst. Sci. Discuss., doi:10.5194/hess-2016-109, 2016
Manuscript under review for journal Hydrol. Earth Syst. Sci.
Published: 9 March 2016

Hydrology and Earth System Sciences
Open Access
Discussions

yield estimates of absolute storage depths (L). Their normalization requires measures for storage capacity of the different catchment subsurface compartments, which should reflect both total and active storage volumes as well as the fractions of free water and capillary bounded water in soil. Estimation of these storage properties is hampered by the unknown depth of the lower boundary of the control volume and the heterogeneity of the subsurface materials (Troch et al., 2003; Spence, 2007; Soulsby et al., 2009). We thus normalize the storage estimators using average root zone field and air capacity, which are available through national soil maps (BGR, 1995). Despite their limitation in the vertical direction, these estimates are deemed to provide an indication of the relative importance of the storage volume containing capillary bounded water, which feeds evaporation and transpiration, and free water feeding groundwater recharge and runoff production (Zehe et al., 2014).

Normalization of rainfall-runoff response and seasonally accumulated runoff is straightforward in the case of capacity controlled runoff production by means of either total rainfall depth of an event or total annual precipitation. Baseflow during dry spells (radiation driven conditions) requires a different normalization based on estimates of aquifer permeability/transmissivity as these control water release. If this information is not available, as in our case, the average soil hydraulic conductivity provides an alternative.

2.1.2 Coherence and quality of integral storage measures

Estimators of water storage such as dynamic storage (dS) (Sayama et al., 2011) depend essentially on the starting point of integration (Pfister et al., 2003). Coherence, in terms of "achieving comparability", of storage time series hence requires that integration in all catchments starts at the same relative storage amount. This could for instance be after significant dry and/or wet periods, when subsurface wetness can be deemed as being either near saturation or near the minimum. Particularly in the case of a strongly seasonal climate, distinct dry and wet periods can be useful in selecting a proper start date.

As dS is i) based on the assumption of a closed water balance and ii) calculated from (areal) estimates of precipitation and model based estimates of evapotranspiration, related uncertainties have a direct effect on the storage estimator. A straight forward quality check of dS is to plot it against normalized accumulated precipitation for several years, using the long term annual mean precipitation for normalization. By comparing patterns of dS for time periods of potentially similar accumulated input one may detect trends, non-monotonic step changes or other inconsistencies. In our case most of the 130 datasets did not pass this benchmark test (compare section 3).

Finally, we face a similar challenge of "when to start" when relating integral storage measures to normalized baseflow. This is because "onset" and "duration" of the baseflow recession may have variable definitions and meanings (Blume et al., 2007). Furthermore, discharge at the river gauge is an aggregation of runoff production, concentration and routing along the river network. These

Hydrol. Earth Syst. Sci. Discuss., doi:10.5194/hess-2016-109, 2016
Manuscript under review for journal Hydrol. Earth Syst. Sci.
Published: 9 March 2016

Hydrology and Earth System Sciences Discussions

processes cover different spatio-temporal scales which make it increasingly difficult to determine a direct relationship of baseflow behaviour to integral storage measures when moving up in scale.

2.2 Candidate storage, response and intensity estimators for baseflow, runoff events and the seasonal water balance

This section introduces normalized storage and runoff response measures, their combination into dimensionless storage/state-response diagrams as well as their statistical analysis. We distinguish among i) the generation of baseflow during radiation driven conditions, ii) rainfall-runoff events as the driven case and iii) the seasonal water balance. The latter is separated into the winter term and the vegetation period, to explore the impact of vegetation controls. Our candidate diagnostic measures for high frequency runoff processes and intensity control are introduced at the end.

2.2.1 Normalized storage measures

Firstly, we use a normalized and re-scaled version of dynamic storage (dS^*) (see Appendix A1 on this aspect). dS^* is calculated as the residual of the water balance equation, using estimates of areal precipitation (P), model based estimates of evapotranspiration (E) and observed discharge (Q). As given in Equation 1 we use the average soil storage volume for normalization, characterised by the sum of effective field capacity (eFC) and air capacity (AC) in the root zone (τ), since metric information on aquifer capacity is not available. Estimates of eFC_τ and AC_τ are taken from the national soil map of Germany (BGR, 1995):

$$dS^*(t) = \frac{\sum_{t=1}^{T} P(t) - Q(t) - E(t)}{AC_\tau + eFC_\tau} \tag{1}$$

dS^* is deemed to represent the total active bulk catchment water storage and we expected it to be associated mainly with deeper storage compartments and hence to control the slower flow processes. Values of dS^* around zero indicate dry conditions whereas values near one indicate that dynamic storage is equal to the root zone storage volume. Note that both values > 1 (e.g. during the occurrence of snow) and < 0 may occur and absolute values must not be interpreted.

The second storage estimator is chosen to better reflect near surface storage. Similar to other studies (Heggen, 2001; Brocca et al., 2009; Graeff et al., 2012) we estimate normalized antecedent moisture (θ^*), which is equal to the difference between precipitation and evaporation totals within the last seven days (T=7 days in Equation 2) normalized again by the average soil storage volume:

$$\theta^*(t) = \frac{\sum_{t=T-7d}^{T} (P(t) - E(t))}{AC_\tau + eFC_\tau} \tag{2}$$

Lastly we use a normalized specific pre-event discharge (Q^*) averaged across the last seven days:

$$Q^*(t) = \frac{\frac{1}{n}\sum_{t=T-7d}^{T} Q(t)dt}{AC_\tau + eFC_\tau} \tag{3}$$

Hydrol. Earth Syst. Sci. Discuss., doi:10.5194/hess-2016-109, 2016
Manuscript under review for journal Hydrol. Earth Syst. Sci.
Published: 9 March 2016

Hydrology and Earth System Sciences
Open Access
Discussions

The main disadvantage of Q^* is that it cannot be attributed to any specific subsurface storage compartment as it inevitably represents a combination of both, storage and release. The advantage is that it relies on the best observation we have.

2.2.2 Baseflow generation during non-driven conditions

To explore controls of catchment structure and storage on baseflow generation we relate specific baseflow depths (Q_b), normalized by the bulk average catchment hydraulic conductivity, to the different storage measures. To this end we define baseflow conditions as follows: ET < 0.1 mm, no occurrence of snow, $\frac{dQ}{dt} < 0$ and no input in $P > 0.1mm$ for a period of at least one, three and five days. The one- and three-day period data sets are used to visually inspect how fast Q decreases after precipitation ceases, which indicates how fast the terrestrial filter properties become dominant. Within our statistical analysis we exclusively consider stream flow data where the last input in $P > 0.1\,mm$ was at least five days ago. For response normalization we use the arithmetic average saturated hydraulic conductivity (Ks) of the catchment (Equation 4), since other estimators for bedrock permeability were not available. Ks is estimated for each catchment based on available grain size distribution using *Rosetta's* pedo-transfer functions (Schaap et al., 2001).

$$Q_b^* = \frac{Q_b}{Ks} \tag{4}$$

Normalized baseflow is then related to dS^* and θ^* using the Spearman's rank correlation coefficient (ρ) and the non-parametric test of significance proposed by Best and Roberts (1975). In the case of significant relations (p-values<0.001), we try to identify an empirical storage-baseflow relationship by fitting power laws using dS^* and θ^* as predictors using *R* (R Development Core Team, 2015). The quality of these relationships are judged by comparing their root-mean-squared-error to the standard deviation of the normalized baseflow values (nRMSE).

Our approach is in line with past attempts to relate stream flow variations and drainage behaviour of hillslopes or catchments (e.g., Laurenson, 1964; Rodríguez-Iturbe and Valdés, 1979; Brutsaert and Nieber, 1977) and searches for feasible storage-baseflow relationships (Kirchner, 2009). Here, we also test the spatial consistency of these storage-discharge relationships by comparing the multiplier in the power law (as estimate of the effective catchment permeability) to the corresponding variation of Ks between the catchments.

2.2.3 Event scale rainfall-runoff response

At the scale of individual rainfall-runoff events we relate event runoff coefficients (CR_E), defined as total event quick flow volume ($\sum Q_E$) divided by total precipitation ($\sum P_E$) (Equation 5), to the different storage measures. To assure comparability of runoff coefficients, as recommended by Blume et al. (2007), and to assure a sufficiently large sample we use an automated detection of rainfall-runoff events based on a modification of the constant-k method (Blume et al., 2007) (details

Hydrol. Earth Syst. Sci. Discuss., doi:10.5194/hess-2016-109, 2016
Manuscript under review for journal Hydrol. Earth Syst. Sci.
Published: 9 March 2016

on the method are provided in A2).

$$CR_E = \frac{\sum Q_E}{\sum P_E} \tag{5}$$

We then select rainfall-runoff events with daily precipitation depth $\geq$ 10 mm and calculate both, coefficients of determination (Pearson) and Spearman rank correlation coefficients among CR_{Es} and the three different normalized storage estimators. Significant relationships are identified by p-values<0.001 in a two-sided t-test or the non-parametric test of Best and Roberts (1975). These are interpreted as evidence for capacity controlled runoff production. In case the respective storage measure were uncorrelated, we test multiple regressions between CR_E and dS^*, Q^* and/or θ^*, respectively.

2.2.4 Storage control on seasonal runoff generation

To shed light on the seasonal dynamics of catchment storage and release we compile normalized annual double mass curves (nDMC) and triple mass curves (nTMC) for different hydrological years. Normalized double mass curves relate cumulated runoff ($cum.Q/\sum P$) to cumulated precipitation ($cum.P/\sum P$). The normalized triple mass curve adds cumulated evapotranspiration ($cum.E/\sum P$) as the third dimension to the plot. The rationale is to check whether the annual water balance is closed within a hydrological year, or whether the system carries stored water into the next year. The winter period and vegetation periods are separated using a temperature index model proposed by Menzel et al. (2003) and analysed separately.

The nDMCs within different catchments are compared according to a) the average and mean absolute deviations of their slopes within the winter and vegetation period, b) the presence and onset of a regime shift marked by plateaus and c) the mean and inter-annual variation of the annual runoff coefficient (CR_{yr}). Regime shifts are further analysed based on the anti-correlation of summer and winter runoff coefficients (CR_S and CR_W) with actual annual evaporation from available water balance simulations. Finally, we attribute differences within the double and triple mass curves to a range of different (n=24) structural and climatic properties of the catchment including temperature sums, characteristics of the grain size distribution, surface cover and several others. Particularly, we test the product of topographic gradient and saturated hydraulic conductivity as an explanatory variable, as they are considered to act in concert.

2.2.5 Intensity controlled runoff generation

Our initial idea was to detect high precipitation rates as those being larger than the estimated hydraulic conductivity and to compare this to peak flow of events normalized with peak intensity of rainfall. To correct for the temporal mismatch between the maxima P and Q, we intended to employ a mean response time defined on the lag cross correlation between P and Q for each individual event (Kirchner, 2009). However, this approach did not yield clear signals due to several likely reasons.

Although hot spots in rainfall intensities are known to be localised and dynamic (Goodrich et al., 1995; Fiener and Auerswald, 2009), we are left having to treat them as spatial rather uniform values due to the low density of rain gauges in our study area. Moreover, texture based estimators using the Rosetta pedo-transfer functions (Schaap et al., 2001) remained as the only option and left us without a proper estimator of the influence of preferential pathways.

To separate high intensive rain showers from low and moderate intensive events we next calculate normalized rainfall event duration (T_E^* (h)) as the ratio of total event rain depth ($\sum P_E$) divided by the maximum observed precipitation intensity ($P_{E,max}$), for all rainfall events exceeding a threshold of 10 mm. The threshold of 10 $\mathrm{mm\,h^{-1}}$ is recommended by the German Weather Service (DWD) to detect strong rainfall events.

$$T_E^* = \frac{\sum P_E}{P_{E,max}} \tag{6}$$

We expect convective, high intensive and extreme rainfall events to cluster at short normalized event durations with a large total amount. Consequently, we relate the maxima in the temporal changes of discharge ($dQ_{E,max}$) and precipitation ($dP_{E,max}$) (both in $\mathrm{mm\,h^{-2}}$) - which implies relating the acceleration of rainfall with stream flow mass. As high frequency processes are characterised by sharp peaks, we expect this normalized and dimensionless intensity change (I_E^*) (Equation 7) to separate intensity controlled from capacity controlled runoff production as intensity controlled conditions cluster at large I_E^*. Note that I_E^* is an intensity measure and thus non-additive. It is independent from the runoff coefficient.

$$I_E^* = \frac{dQ_{E,max}}{dP_{E,max}} \tag{7}$$

Both, the normalized event duration and the normalized maximum change in stream flow are jointly analysed within scatterplots. Here, we expect intensity controlled processes to cluster around small values of T_E^* and large values of I_E^*. Additionally, we compile three-dimensional scatterplots using $\sum P$, $dP_{E,max}$ and $dQ_{E,max}$ on the x, y and z-axis respectively. Here we expect high $dQ_{E,max}$ to be associated with high $dP_{E,max}$ whereas $\sum P$ is deemed to be unimportant.

3 Study area and dataset

The feasibility of the above introduced signatures is tested by inter-comparing operational data from the Bavarian Environmental Agency (LfU) for 130 catchments located in the Bavarian Danube basin ($\approx$ 45.000 km^2). In section 3.2 we detail the differences in the climate and physiographic setting of our test catchments and present our perception of the dominant hydrological processes. Before that, we will briefly discuss the quality of the database, which in fact was in most catchments so poor that the majority of the sites had to be excluded from the analysis.

3.1 Data quality and selection of headwater catchments

We focus on lower mesoscale catchments to minimize routing effects and select all gauged headwater sites $\leq 170\,\mathrm{km}^2$ within the Bavarian part of the Danube basin. For this, hourly hydro-meteorological time series from the period 01.11.1999 until 31.10.2004 are available. The data base in the resulting 130 catchments is analysed according to a set of different quality criteria. We only include catchments where i) at least one meteorological station was closer than 20 km, ii) the total absolute water balance error was smaller than 5 % , iii) the amount of missing and/or implausible meteorological data was < 5 %, and iv) where the streams are not subject to any severe regulation. This screening resulted in only 22 catchments being classified as suitable for the analysis. The sites are spread across the Bavarian part of the Danube basin (Fig. 1 and Appendix A3).

– Figure 1: MAP STUDY SITE –

The densest coverage in meteorological stations was for precipitation with a total number of 244 stations. The coverage of the other meteorological variables was much coarser, with 59, 55 and 43 stations for temperature, humidity and radiation, respectively. Since these numbers include stations which are up to 20 km apart from the finally selected 22 headwater catchments, we even tolerated lower densities in meteorological stations as e.g. in the Mopex data set (Schaake et al., 2000; Duan et al., 2006). The lowest densities of meteorological stations are located in the southern alpine areas and the corresponding foothills and in the north-eastern parts of the Bavarian Danube catchment. Catchment characteristics were derived from different digital map products of Germany such as for soil (scale: 1:1,000,000) (BGR, 1995), hydrogeology (scale: 1:1,500,000 and 1:500,000) (Duscher et al., 2015; BGR and SGD, 2015) and geology (scale: 1:1,000,000) (Toloczyki et al., 2006), a digital elevation model with resolution of 25 m, the CORINE land use data (as of 2006) and the official stream network provided by LfU. Last but not least, we employed the conceptual hydrological model LARSIM (Ludwig and Bremicker, 2006) as it provides consistent areal estimates of evaporation, rainfall and snow water equivalent. LARSIM has been calibrated for all study catchments and operates at hourly time steps. Evaporation is simulated using the Penman-Monteith equation. Model input is based on interpolated station data (grid point method, US Department of Commerce, 1972). Additional information on the Bavarian part of the Danube basin, the hydro-meteorological data and the Larsim model can be obtained from Seibert et al. (2014).

3.2 Landscape setting and perceptual models of runoff generation

Topography, landuse, geology, soil and aquifer properties are highly variable among the different headwaters of the Bavarian part of the Danube basin, as the region was unequally covered by ice during the last ice age. The remaining 22 catchments reflect the entire physiographic range (see Tables 1 and 2). This is underpinned by the large range of topographic gradients (ϕ) (Table 1) calcu-

Hydrol. Earth Syst. Sci. Discuss., doi:10.5194/hess-2016-109, 2016
Manuscript under review for journal Hydrol. Earth Syst. Sci.
Published: 9 March 2016

lated according to McGuire et al. (2005) as the flow path length from each pixel to the stream divided by the corresponding difference in height using the Whitebox geographic analysis toolbox (Lindsay J.B., 2014). The climate gradient is also rather strong with mean annual precipitation (MAP) ranging from 600 mm in the northern sub-catchments to more than 2000 mm in the southern, alpine areas and a total average of 1000 mm. Annual potential evapotranspiration ranges from 350 to 600 mm. Both P and E regimes are characterized by distinct seasonal cycles. In some of the southern alpine areas more than 50 % of the precipitation may fall as snow.

Based on the dominant physiographic properties (referencing to Table 1 and 2) we grouped the 22 catchments into 5 major classes, which largely rely on (hydro)geology and detail on the expected dominant processes drawing from Peschke et al. (1999) and Schmocker-Fackel et al. (2007), which are categorized into being capacity controlled or intensity controlled:

- The "Alpine sites" (ALP) in the very south are dominated by poorly developed and shallow soils (average root zone depth $\leq$ 35 cm) with high contents of skeleton and coarse material (average pore volume 110 mm, $Ks \approx 1e-6\ m\ s^{-1}$) over highly productive fissured (partly karstified) aquifers. The surface cover is sparse with a clear dominance of forests and meadows. Rock outcrops occur, particularly above the tree line which is approximately around 1800 m.a.s.l in this environment. Catchments of this physiographic region (ALP1 . . . ALP4, n=4) exhibit strong geopotential gradients (median $\phi = 0.36$) and receive about 1500 mm annual rainfall. These characteristics clearly suggest a dominance of rapid flow paths i.e. surface runoff, pipe flow/by-passing and rapid sub-surface stormflow. Here, we might thus expect high frequency, intensity controlled runoff formation, at least during extreme conditions.

- The "Triassic catchments" (TRI) (n=3) are composed of well-drained, poor to moderately developed sandy soils (mean root zone depths of 50-80 cm) with high portions of coarse material. Regosols, rendzinas, cambisols and partly podzols with rather weak vertical differentiation over calcareous sandstone (TRI1, TRI2) and sandstone (TRI3) prevail. The parent material sustains moderately to highly productive pore and fissured aquifers. The land use is dominated by arable land (about 60 %). Long-term mean annual precipitation is around 750 to 800 mm. The median gradients within the three catchments differed slightly between 0.028 and 0.038 (-) which is an order of magnitude smaller than in the alpine areas. These characteristics suggest a perceptual model, where subsurface matrix flow dominates, and the aquifer strongly controls runoff generation. However, coarse substrates and corresponding structures may also sustain rapid flow paths and saturation excess during high intensity rainfall events.

- The faulted "molasses basin" (MOL) and adjacent transition areas belong to a heterogeneous region which hosts seven of our sites on mostly well developed, medium and deep cambisols (root zone depths > 70 cm) with high contents of aeolian sediments (silt and loess). The parent material is often composed of sheet gravel (MOL1, MOL2, MOL3, MOL5) and sedimentary rock and fluvial sediments (MOL4, MOL6, MOL7) which predominantly sustain low to moderately productive aquifers. In these catchments pore volumes are partly well above > 300 mm. The soils are fertile which promotes an intensive agricultural use. The surface topography is characterized by soft hills and U-shaped valleys. The corresponding gradients in geopotential are weak. Therefore, we expect that sub-surface capacity controlled (matrix) flow is the dominant runoff process. However, during high intensity rainfall Hortonian overland flow (due to surface crusting on arable land) and saturation overland flow due to reduced hydraulic conductivity is deemed to create a mixture of capacity and intensity controlled runoff formation.

– The catchments in the "Bavarian Forest" (BFO) (n=3) consist of loamy, partly sandy cambisols with comparably high contents of skeleton (in some areas up to 75 Vol.-%). These lie over crystalline granite and gneiss which are fractured but practically non-aquiferous rocks. The root zone depth is on average 60 cm. Forests and meadows cover 60 to 90 % of the surface. The topography is more pronounced and median gradients reach values up to 0.08. In these areas we expect that preferential flow pathways contribute significantly to runoff generation, but merely in a capacity controlled manner.

– The data set also includes four catchments from the "Alpine Foreland" (AFO1...AFO4). Like the MOL-area this region exhibits complex characteristics as it was altered by three different glacial advances (and retreats). Consequently, we observe high spatial variations in the geological parent material and thus, also in the soils, land use and hydrological characteristics (see Table and 1 and 2). The same applies for topography, as it is a relict of the different glacial periods. The relief, though composed of similar gradients as e.g. the Triassic or Molasse sites, includes a rich variety of landforms typically found on ground, end and lateral moraines such as rolling foothills, (glacial) lakes, swamps and smaller surface water courses. Hence, there is no single dominating perceptual model on runoff formation available. Also the importance of different storage compartments cannot be estimated for this region as a whole, but needs to be evaluated individually for each site.

To further illustrate variations in the seasonal water balance, we present regime curves for four different catchments (Fig. 2). The catchment TRI1 (Fig. 2, top left) receives a fairly constant input in P throughout the year, but releases Q with a strong seasonality and pronounced minimum during summer. Compared to the other sites the inter-annual variation in E is rather large. The catchment AFO4 (Fig. 2, top right) in contrast shows seasonality in P but a fairly constant output in Q. ALP4 (Fig. 2, bottom left) and ALP2 (Fig. 2, bottom right), which are both alpine sites, show a pronounced minimum in Q during February due to snow storage. ALP2 however shows a very large range in both P and Q during summer, which suggests little buffering and a high reactivity. In contrast, ALP4 has a much more damped response to P during summer and a more pronounced seasonality in ET.

– FIGURE 2 KERNEL DENSITY ESTIMATES –

4 Results

The following section documents the performance of our diagnostics. More specifically, we present selected dimensionless storage/-state-response analyses that corroborate either their feasibility or their failure in discriminating differences in runoff behaviour in combination with the selected statistical measures introduced in section 2.2.

4.1 Storage and structure control on baseflow generation

During low flow conditions, the storage estimators dS^* and θ^* are in most cases linearly independent. Table 3 presents the corresponding statistics. However, significant relationships are encountered in 7 out of 22 cases, with the highest Spearman rank correlation coefficient (ρ) between dS^* and Q_b^* is 0.39 with an average of 0.07. All catchments except one have high and significant rank coefficients of determination between dS^* and Q_b^* with values ranging from 0.12 to 0.88 and an average of 0.59. Hence, dS^* seems to be a valuable predictor for low flow in a rather wide range of environmental conditions. We also find significant relationships between θ^* and Q_b^* in about 50 % of all cases but with rank correlation coefficients being all smaller than 0.28 (except for catchment AFO2, were ρ was 0.54). Hence, θ^* possesses much less predictive power.

– Table 3: STATISTICS OF NON-DRIVEN CONDITIONS–

Five catchments (MOL5, MOL4, TRI1, MOL1, BFO3, MOL7) reveal power model exponents close to 1 ± 0.3 for their estimated normalized storage-discharge relationship (Table 3). This corroborates a linear storage-baseflow relationship in line with Fenicia et al. (2006). For the remaining catchments, we obtain exponents clearly different from 1, suggesting a non-linear interplay of storage and baseflow production in the majority of the catchments. This finding is also supported by 2D scatterplots (Fig. 3) which clearly show a strongly non-linear relationship between dS^* and Q_b^* at e.g. AFO3, MOL6, MOL2, BFO1, JUR1 and other sites. The nRMSE of the estimated storage-baseflow relations was on average 0.74, with best values of 0.43 and worst values larger than 1. Hence on average, the storage-discharge relationships are a better predictor than the average Q_b^*. Furthermore, we do not find a distinct spatial pattern in the exponents as both cases (linear and non-linear) occurred throughout different geologies and climate settings.

The normalized baseflow is in fact the flow multiplied with the inverse of the conductance. Due to the gradient-flux relationhip we thus expect the multipliers in the normalized storage discharge relationship to partly reflect the strength of the gradient driving baseflow production. In line with this we find that the median of the catchment gradients explains ($r^2 = 0.28,\ p = 0.023$) of the multipliers when leaving out two alpine sites.

– FIGURE 3: EMPIRICAL STORAGE-BASEFLOW RELATIONSHIP –

Hydrol. Earth Syst. Sci. Discuss., doi:10.5194/hess-2016-109, 2016
Manuscript under review for journal Hydrol. Earth Syst. Sci.
Published: 9 March 2016

Hydrology and Earth System Sciences
Open Access
Discussions

4.2 Storage control on rainfall-runoff response

The total number of rainfall events within the four year period (n=14854) ranges from 334 to 859 among catchments. Omitting those influenced by snow or triggered by rainfall totals smaller than 10 mm yields 1174 rainfall events (53 events per catchment on average). The distribution of the corresponding CR_E is right skewed with a median CR_E of 0.06, a mean of 0.11 and a maximum value of 0.83 (inter-quartile range = 0.13).

Table 4 presents the resulting statistics of the analysis of the driven case. Significant rank correlations among the CR_E and the three storage measures dS^*, Q^* and θ^* are found in 9, 15 and 8 out of 22 cases, respectively. The corresponding average ρ values are 0.61, 0.63 and 0.52, respectively. In all cases where dS^* is significantly correlated to CR_E, Q* is significantly correlated to CR_E as well. Basically the same applies for the comparison of Q^* and θ^*. Whenever θ^* is significantly correlated to CR_E, Q^* is significantly correlated to CR_E as well, except for the catchments ALP1 and ALP4. We may thus state that Q^* is the best predictor for CR_E with both the highest number of significant cases and the highest ρ values.

– Table 4 STORAGE STATISTICS OF DRIVEN CONDITIONS–

Furthermore, we find a rather interesting regional pattern where a distinct storage measure performs much better. Q^* is consistently not (significantly) correlated to CR_E in the four alpine sites while θ^* has significant ρ values in three of the four catchments. Consistently with this, plots of CR_E versus θ^*, thereby scaling the point size with rainfall depth, clearly corroborate the dominant influence of rainfall depth (and probably intensity) in the Alpine catchments (e.g. ALP4, Fig. 4, top left) (see also section 4.4). A remarkable finding from the Triassic catchments is that the three catchments TRI1, TRI2 and TRI3 have the highest ρ and r^2 values between CR_E and Q^* among the entire data set, with up to 70 % of explained variance (compare Table 4). Relationships between CR_E and θ^* are often pretty linear here, whereas that between CR_E and dS^* indicates threshold behaviour (see Fig. 4, top right). Also the catchments located in the Molasse area often show significant ρ values between CR_E and Q^* and the functional relationship is linear in most cases (e.g. MOL5, Fig. 4, bottom left). However, the relationships are clearly more noisy than in the Triassic area. The catchments located in the Bavarian forest have rather similar ρ values for both, dS^* and Q^* and the functional relationship appears linear as well (see e.g. BFO3, Fig. 4, bottom right).

– FIGURE 4: STORAGE CONTROLS ON EVENT RUNOFF COEFFICIENTS (4x1) –

The inter-comparison of the storage measures at the beginning of the rainfall-runoff events reveals dS^* and θ^* as being not significantly correlated, except for one catchment (MOL5) (Table 4). However, Q^* is significantly correlated to dS^* in 14 and to θ^* in 12 out of 22 cases, although the catchments do not coincide. The statistics also reveal that multiple linear regressions among CR_E and the two most explanatory and uncorrelated storage measures explain - at best - 5 % of additional

Hydrol. Earth Syst. Sci. Discuss., doi:10.5194/hess-2016-109, 2016
Manuscript under review for journal Hydrol. Earth Syst. Sci.
Published: 9 March 2016

variance (r^2) in all except three catchments (ALP3, ALP2, MOL7) compared to the univariate regressions. Hence, we conclude that the consideration of different uncorrelated storage measures does not further improve the predictability of the event runoff coefficients compared to the single best predictor.

Similar to the non-driven case we tested for significant relationships between average and median CR_E and Ks times ϕ. The resulting coefficients of determination are very small in all cases ($r^2 \leq 0.02$). Also the three regression slopes between CR_E and the different storage measures obtain small and insignificant coefficients of determination. However, it turned out that the median topographic gradient alone explains 31.4 % (p-value=0.0066) of the variance of the average CR_E between the catchments. We may state that gradient and resistance are conjunct during baseflow recession when the system operates close to local equilibrium conditions. During rainfall conditions the gradients dominate the concert, which indicates further-from-equilibrium conditions.

4.3 Seasonal interplay of storage and release

4.3.1 Normalized double mass curves

The double mass curves are similar in all catchments in terms of a fairly linear increase in the winter period and a clear regime shift towards much flatter, partly zero slopes in the vegetation period. In fact the slopes of the nDMCs are almost constant, just parallely shifted, during the period of vegetation at many sites (e.g. at MOL2, TRI3 or BFO1, Fig. 5, top left, top right and bottom right, respectively). Strikingly, the onset of the vegetation period, defined by a temperature index model (Menzel et al., 2003) accurately predicts when the regime shift occurs (in terms of $cum.P/\sum P$). Moreover, temperature sums explain 70 % of the variance of the summer runoff coefficients with respect to the entire range of our physiographic setting. During winter, temperature aggregates are not significant and without predictive power (Fig. 5, bottom right). We may thus state that the onset of the vegetation period dominates the seasonal interplay in storage and release during the "summer" period, in all of our physiographic and climatic settings (except for the alpine region).

– FIGURE 5: nDMC AND SCATTERPLOT CR vs. TEMPERATURE SUMS –

The different catchments within our data set show considerable variations in the seasonal summer and winter runoff coefficients and partly also with respect to their inter-annual variation (Table 5). On average the seasonal winter runoff coefficients ($CR_W = 0.67$) exceed the average summer runoff coefficients ($CR_S = 0.32$) by a factor of 2, with two exceptions (ALP2 and ALP3, both alpine sites). The mean absolute deviation (mad) of the seasonal runoff coefficients are twice as large during winter ($mad_{CR_W} = 0.1$) as during summer ($mad_{CR_S} = 0.06$) (Table 5).

– TABLE 5: STATISTICS AND SLOPES OF THE nDMCs –

With respect to the different physiographic settings we encounter distinct seasonal and spatial patterns. During winter the highest average nDMC slopes ($CR_W = 0.8 - 0.9$) occur in the north eastern catchments (BFO1, BFO2, BFO3) which are rather densely forested, but also in the alpine ALP1 catchment. ALP4, ALP3 and ALP2, which are also alpine catchments and located on similar altitudes, show much lower winter runoff coefficients of 0.64 to 0.71 on average, probably due to storage in the snow pack. The smallest winter runoff coefficients (0.35 and 0.55) occur in MOL7 and TRI3, respectively. With respect to the inter-annual winter variance we encounter small mean absolute deviations ≤ 0.05 in low lying sites of the Molasse and glacial drift areas e.g. MOL5, AFO4, AFO2, AFO1. High mean absolute deviations ≥0.15 occur in different geologies, including the sites TRI2, BFO1, JUR1 and BFO3. Please also note that $CR_{yr} > CR_W$ in a few cases where snow exhibits a strong control on winter runoff regimes (e.g. ALP3 or ALP2, see Table 5). Here, fitting linear regressions to the double mass curves is not suitable for estimating seasonal winter runoff coefficients.

According to the statistical analyses in which we regressed 24 different variables against the slopes of the seasonal winter runoff coefficients, the most explanatory variables are sand content ($r^2 = 0.29$), median gradient (ϕ) times Ks ($r^2 = 0.22$), silt content ($r^2 = 0.22$), forest coverage ($r^2 = 0.16$), skeleton content ($r^2 = 0.15$), number of frost days ($r^2 = 0.14$), effective field capacity ($r^2 = 0.13$) and absolute sum of negative temperatures ($r^2 = 0.12$). All other variables have coefficients of determination $r^2 \leq 0.10$. In several multiple linear regressions based on the above mentioned variables the best result is achieved for a combination of ϕ times Ks, forest cover and absolute sum of negative temperatures (multiple $r^2 = 0.30$, p-value<0.001). Active storage estimates (dS), summer temperature sums and length or end of the period of vegetation from the previous hydrological year do not help to improve the prediction of the actual CR_W. The key finding in this analysis is that ϕ times Ks yields a $r^2 = 0.22$, whereas two variables alone only explain 0.02 and 0.08 % of the variance in the CR_W, respectively. This corroborates that surrogates for gradients and resistances act jointly and that their impact is detectable even at the lower mesocale.

The summer season is characterised by an opposite spatial pattern compared to the seasonal winter runoff coefficients. The highest seasonal $CR_S \geq 0.8$ is found in the snow-dominated alpine catchments of ALP3 and ALP2. The smallest CR_S with values between 0.07 and 0.12 are encountered at the Triassic sites (TRI3, TRI2, TRI1). It is also important to note here that several low-lying sites the CR_S shows very little inter-annual variance as indicated by mean absolute deviations ≤ 0.03 (e.g. MOL5, TRI3, TRI2, MOL6, MOL2, MOL4, JUR1, MOL3 and others) (Table 5). In these catchments the slopes of the nDMCs are fairly constant throughout different hydrological years indicating a very strong control of evapotransiration on the water balance during summer. At these sites the curves of the nDMCs in summer have nearly identical slopes and are simply shifted in parallel depending on the onset of vegetation activity.

Hydrol. Earth Syst. Sci. Discuss., doi:10.5194/hess-2016-109, 2016
Manuscript under review for journal Hydrol. Earth Syst. Sci.
Published: 9 March 2016

We may hence state that normalized double mass analyses are powerful tools for discriminating seasonal differences in the interplay of storage and release among mesoscale catchments. However, they do not provide insights into the reasons for inter-annual variations. In several cases we observed inter-annual variations in $CR_{yr} \geq 0.1$, which could stem from variations of P or ET or a carry over of water storage into the next year. To provide more insights we introduce normalized triple mass curves by adding $cum.E/\sum P$ as a third dimension.

4.3.2 Normalized triple masse curves

Conceptually we usually assume that the change in storage tends to zero within a single hydrological year. Hence, we assume that large inter-annual variations in the rainfall-runoff ratio CR_{YR} coincide with large inter-annual variations in the evapotranspiration ratio (CE_{YR}). To evaluate this assumption on our data set we construct normalized triple mass curves and calculate the mean absolute deviation for both, CR_{YR} and CE_{YR}. Within our sample we find several catchments where the mean absolute deviation in the evapotranspiration ratio ($mad_{CE_{yr}}$) is rather similar to the mean absolute deviation in the annual runoff coefficients ($mad_{CR_{yr}}$) e.g. MOL5, MOL2, ALP1, MOL4, or MOL1 (see examples in Fig. 6, upper row). However, we also find several sites where $mad_{CR_{yr}}$ clearly exceeded $mad_{CE_{yr}}$ e.g. TRI3, TRI2, BFO1, JUR1, BFO3 or BFO2 (compare Fig. 6, lower row). This may be attributed to a carry over of water storage feeding runoff formation (blue water) between the hydrological years, indicating inter-annual memory (under the assumptions of a closed control volume). Only in two catchments (AFO4 and MOL7) $mad_{CR_{yr}}$ is substantially smaller than the corresponding $mad_{CE_{yr}}$. This can be explained by a carry over of water into neighbouring years, feeding ET (green water).

– FIGURE 6: , nTMCs: ALP1, MOL2, TRI2, BFO1 –

4.4 Intensity controlled runoff formation

4.4.1 Data evidence in Alpine catchments

Strikingly, we also find signatures of intensity controlled runoff in two Alpine catchments (ALP1 and ALP2). This is illustrated in Fig. (7) which compares two flood events from site ALP2 caused by rather similar totals of rainfall (244 and 200 mm) and identical event runoff coefficients ($CR_E = 0.58$). The rainfall intensities as well as the discharge peaks in the right panel are however twice as large compared to the left panel, yielding considerable differences in the normalized temporal intensity changes ($I^*_E = 0.08$ vs. $I^*_E = 0.32$). Similar rainfall-runoff dynamics with strong temporal changes in P which are followed by strong increases in Q are observed during many events at site ALP1.

– Figure 7: OBSERVED EVENTS –

In these catchments the highest normalized temporal intensity changes indeed cluster at small normalized event durations (Fig. 8, left panel). The same scatterplot for MOL2 (Fig. 8, right panel) reveals normalized temporal intensity changes to spread equally across all event durations. The three-dimensional scatterplots of normalized temporal runoff changes against total precipitation and maximum intensity (Fig. 8, lower row), reveal clearly that large runoff changes coincide partly with high intensities and small rainfall totals. We may, hence, state the proposed signatures are feasible for detecting high frequency runoff even within low frequency data sets in mesoscale catchments. To illustrate that this is of more than academic importance we present a comparative model exercise.

– Figure 8: INTENSITY MEASURES –

4.4.2 Explorative modelling for intensity limited runoff formation

We compare two different model concepts to further elaborate the feasibility of our diagnostics for detecting intensity control. Our comparison shall particularly highlight the errors we might expect when simulating intensity controlled runoff formation with models relying on capacity controlled runoff formation with respect to the events depicted in Fig. 7. Specifically, we compare the HBV beta store (Bergstroem, 1976) with a Green and Ampt approach (G&A) using the solution of Peschke (1985), as typical concepts for capacity and intensity controlled runoff formation. Both runoff generation concepts are implemented in R (R Development Core Team, 2015) and combined with a simple linear reservoir, whereas surface runoff is allowed to bypass the latter in the case of G&A. Both implementations are then fitted to observed stream flow data in an event based mode. Here we optimize the maximum storage depth ($SMax$), beta parameter (β) and the reservoir constant (k_{res}) in the case of HBV using a simulated annealing algorithm in combination with the root-mean-squared-error as objective function. The G&A approach is parametrized based upon a Rosetta Schaap et al. (2001) estimate of Ks and a literature value for the suction head (psi) at the wetting front (Maidment, 1993). The parameters of the linear reservoir ($SMax$ and k_{res}) are adopted from the HBV optimization to ensure identical conditions.

During both events depicted in Figure 9 the HBV type setup outperforms G&A, when being judged on the Nash-Sutcliffe-Efficiency (NASH) criterion. During intensity controlled conditions the HBV bucket concept however clearly fails to reproduce the high runoff frequencies in terms of the slope of the rising limb and in the peak discharge (compare black box in Fig. 9, right panel). A closer look at the right panel reveals, however, that G&A matches the magnitude of peak discharge (which is important for flood warning) much better than the beta store model. The slightly worse NASH value is because the timing error in peak occurrence is punished, which is a well known deficiency of the NASH statistical analysis (Seibert and Ehret).

– Figure 9) modelling of intensity controlled processes –

This exercise suggests that we are much better off in capturing sharp peaks of high frequency, intensity controlled runoff formation processes when using model concepts that are sensitive to the controlling, intensive properties compared to model concepts which do not account for this issue. Though this is essentially not new, data driven diagnostics which assist in deciding whether intensity controlled processes need to be considered in hydrological modelling are novel and rarely available.

5 Discussion and conclusions

In this study we propose various dimensionless diagnostics to characterize differences in terrestrial runoff production of catchments at the seasonal and the event scale. Particular emphasis is on a) their suitable normalization and b) on the question whether low-passed rainfall-runoff data from mesoscale catchments still bear detectable signals of high frequency, intensity controlled runoff production. As benchmark we use operational rainfall-runoff data from 22 catchments spread across a wide range of physiographic and climate conditions in the Bavarian part of the Danube catchment.

5.1 Normalized double mass curves discriminating seasonal runoff behaviour

Normalized double mass curves turn out to be an easy-to-compute, yet very powerful means to detect similarity and differences in the seasonal water balance. In our case their general shape is (invariantly) characterized by a linear increase in the winter period and a regime shift with small near to zero slopes when vegetation starts to control the water balance. The onset and duration of this regime shift could be predicted very well by a simple temperature index model (Menzel et al., 2003). In line with this, temperature explains 70 % of the variability of the summer runoff coefficients within the 22 catchments. It is noteworthy that the usual (Gregorian) definition of spring and fall onset are of little help to predict the regime shift here. We hence conclude that vegetation exerts first-order control on stream flow generation in "summer", while onset and end of the summer (i.e. the vegetation period) is defined by temperature conditions rather than simply by the Gregorian day. This finding is important as it suggests that phenological data (and corresponding surrogates) provide valuable information which is mostly not included in standard hydrological data (or at least hardly considered). We further conclude that any assessment of the "pure abiotic controls" of the catchment water balance should be restricted to (snow free) periods of the dormant season.

The variability of winter runoff coefficients is generally much less predictable by the available structural and climatic descriptors. Also the different storage estimators are of little use. The most interesting finding is that the rather coarse estimates of the catchment soil hydraulic conductivity and the median gradient operate indeed as a group and that their impact is even detectable at lower mesoscale sites: their product explains 22 % of the variance in the winter slopes, while either of the values itself is an insignificant predictor. Expressing runoff by the product of an effective gradient

Hydrol. Earth Syst. Sci. Discuss., doi:10.5194/hess-2016-109, 2016
Manuscript under review for journal Hydrol. Earth Syst. Sci.
Published: 9 March 2016

and a control volume conductance, requires the system to operate close to local thermodynamic equilibrium conditions. We hence conclude that this is at least partly the case at the seasonal scale.

Also normalization of the double mass curve is straight forward. Here we use annual precipitation totals of the respective hydrological year. The advantage is that both axes are normalized to one. The disadvantage is that the same amount of relative accumulated rainfall does not correspond to the same total rainfall amount. This would require us to normalize precipitation and discharge with the long term mean annual precipitation at the prize, that the maximum ordinates would then not be constrained to one.

We also provide evidence that normalized triple curves are well suited for explaining inter-annual variability of annual runoff coefficients either by different accumulated evaporation totals or by carry over in storage. The drawback of this signature is that it needs a calibrated water balance model for its calculation, due to the required estimates of E, while the double mass curve relies exclusively on standard observables.

5.2 Pre-event discharge as best predictor for capacity controlled runoff production

At the event scale we compare plots of event runoff coefficients against the three partly independent storage estimators i) normalized dynamic storage dS^*, ii) accumulated normalized discharge Q^* and iii) the normalized difference between antecedent precipitation and evaporation, θ^*. Generally Q^*, though it is the less sophisticated measure, does clearly outperform the other storage measures in terms of the explained variances and with respect to the number of catchments with significant rank correlations. Yet the comparison of different storage measures reveals regionally specific dominances. Particularly for the alpine catchments, Q^* is insignificant while antecedent wetness explains most of the variance within three out of four alpine catchments. This is in line with our perception that these basins are composed of shallow soils and we thus expect a higher importance of the near surface storage.

Another interesting finding is that the median topographic gradient explains 31 % of the variability of the mean catchment event runoff coefficient averaged over all 22 catchments. In fact we find the same result for the 90 % quantiles of the runoff coefficients and when using the square root of the topographic gradient. We hence conclude that this correlation reflects fairly well the strong dependence of rainfall totals and intensity on elevation (and the gradient) rather than the influence of the topographic gradient as a force for driving runoff concentration during rainfall driven conditions.

In comparison to Q^* and θ^* and with regard to the effort of its derivation, normalized dynamic storage provides little additional value. Thereupon, dS^* is significantly correlated to Q^* in 14 out of 22 catchments, although it is to be expected that parts of these correlations are spurious (Pearson, 1897; Kenney, 1982), as both, Q^* and dS^* are calculated upon the same variable. Similarly, we argue that correlations between dS^* and response measures such as event runoff coefficients are more difficult to evaluate as they may also involve (non-trivial) spurious fractions because both variables are again calculated based on discharge and precipitation. Partly, this applies for Q^* and θ^* as well, but certainly to a lower degree. We hence conclude that dS^* is of limited use for explaining rainfall driven runoff formation compared to the well known pre-event discharge and the well known antecedent precipitation. We furthermore conclude that these different storage measures characterise storage in different depths, and that event runoff production is controlled by different storage compartments in different regions.

Our results corroborate that the event runoff coefficient is a useful and easy to calculate normalized response measure to discriminate capacity controlled runoff formation. However, it fails to discriminate high frequency runoff production processes as underlined by our findings in the alpine catchments ALP1 and ALP2. We also conclude that normalization of different storage estimators is generally helpful to compare their sensitivity ranges, even when relying on such simple estimates as the root zone storage depth or the pore volume therein, as done here.

5.3 Heterogeneous performance of storage-baseflow relations

The occurrence of 19 (out of 22) significant relations between dS^* and Q_b^* confirms that dS^* is a meaningful storage measure for the prediction of low flow conditions under a range of different (humid) physiographic settings. We also found specific storage-baseflow relationships by fitting power laws, with their exponents and factors being sensitive to changes in the physiographic setting. This finding is in line with the results of Shaw and Riha (2012) who derived storage-discharge relationships for several catchments of up to 6400 km^2 in size using an adaptation of the method proposed by Kirchner (2009).

A closer look reveals however that the estimated storage-baseflow relations are only partly of convincing quality. In many places they are rather noisy despite the fact that the nRMSE suggests predictive power. This corroborates that visual inspection of such relations is indispensable before using them for instance to parametrize regional baseflow production in a model. Parts of the noise in the relations most likely arise from the inherent data uncertainty. However, normalization of dS^* by the root zone storage volume and of Q_b by Ks is also error prone. Ks is at best a surrogate for the aquifer conductance and thickness. The soil map (BGR, 1995) suggests that e.g. BFO1 and TRI1 have identical Ks values (according to Rosetta estimates (Schaap et al., 2001)). However, the hydrogeological map (Duscher et al., 2015) reveals that the aquifer underlying BFO1 is composed of virtually all non-aquiferous fissured rock, whereas the subsurface of TRI1 hosts low to moderately productive pore aquifers (compare Table 2). The alpine sites show similar contradictions as the smallest Ks values coincide with the highest productive aquifer types (still Table 2). A more meaningful structural normalization of Q_b^* would thus require estimates of aquifer transmissivity. We hence conclude that the identification of catchments with similar baseflow production was not feasible with the proposed approach.

Within our attempts to explain differences in the power law multiplier based on catchment characteristics, we derive ϕ based upon surface topography and not, as ideally required, upon bedrock topography. Nevertheless, we find that a considerable portion of the variability is explained by the topographic gradient, in line with the flux–gradient–conductance relation. Given the large number of significant relationships between Q_b^* and dS^* we conclude that dS^* is a feasible predictor for baseflow production within a rather wide range of physiographic settings. This supports our initial assumption that dS^* characterises deep storage.

5.4 "Edge filtering" of low-passed data to detect high frequency runoff processes

The proposed intensity signature detects evidence for high frequency intensity controlled runoff generation in two alpine catchments within the available low frequency data sets. The key is to "edge-filter" both rainfall and discharge data by taking their temporal derivatives and then to normalize the maximum runoff change by the maximum in precipitation change. This response measure separates the available rainfall-runoff events into subsamples with high normalized temporal intensity changes clustering at small event durations. We conclude that the approach we present is an easy-to-apply technique to test for the occurrence of intensity controlled runoff generation processes. This is also relevant for hydrological modelling as we show that a wrong conceptualization of intensity controlled runoff by a capacity controlled model approach might imply that the model misses the flood peak (even though it has a good NASH statistic). Thus, data driven signatures on high frequency intensity controlled runoff generation can assist in the conceptualization of hydrological models or serve as structural benchmarks. We hence conclude that high frequency runoff production might play a much more prominent role in lower mesocale flood production than we usually conclude from analysing hourly (or even lower) resolution data sets. Therefore, we recommend that operational data should be recorded and stored with at least 5 min resolution, as this might reveal high frequency processes operating even more frequently than we expect.

5.5 Conclusion and Outlook

Overall, we recommend the following signatures as suitable to discriminate differences in terrestrial runoff production in lower-mesoscale catchments:

- Normalized double mass curves for the seasonal water balance,
- the event runoff coefficient in relation to pre-event discharge for capacity controlled runoff formation,
- the event duration in combination with the normalized intensity change for detecting high frequency processes.

The onset and termination of the vegetation period are useful to explain differences in the summer water balance. We also argue that gradients and conductances - and hence their underlying controls

- are not independent if one attempts to explain functional differences by differences in the physiographic and climate setting. However, despite the good explanation we found for differences in the summer water balance, we were not able to robustly link functional similarity to structural similarity, based upon the properties available within our (operational) data set.

This brings us to our last conclusion which is founded on the dilemma of quantity vs. quality. On the one hand, inter-comparison studies require large sample sizes to include a sufficient number of end-members and to avoid type I errors (false hits). This makes widely available operational data sets indispensable (at least for the moment). On the other hand, we need accurate and sufficiently resolved data beyond rainfall and runoff to avoid type II errors (false negatives). Such data are (at least for the moment) only included in "research" data sets which are fairly limited in number and spatial distribution. To increase confidence in the proposed signatures we suggest they be applied to i) to a larger number of catchments and ii) to a (nested) set of small and densely instrumented catchments with homogeneous geological setup.

Appendix A

A1 Re-scaling and consistency of integrative storage measures

To ensure that two catchments at least potentially store the same amount of water and start with a similar storage amount, we define the starting point of integration of dS^* using seasonal criteria. Therefore, we first plot dS^* against accumulated annual precipitation normalized by the long-term mean annual precipitation (MAP) (Fig. 10). This helps to compare states with similar potential accumulated input. Next, we re-scale the ordinate such that the origin corresponds to the mean of the local periodic minima, assuming that the soil moisture is near the permanent wilting point at these times. This way we gain a dimensionless estimator for the total active bulk catchment water storage. Values in dS^* of around zero indicate dry conditions whereas values around 1 indicate that dynamic storage is equal to the root zone storage volume. Note that both values > 1 (e.g. during the occurrence of snow) and values < 0, may occur and that absolute values must not be interpreted. Please note, that we encountered significant trends and erratic fluctuations in dS^* in the majority of all sites.

– FIGURE 10: coherent normalization of integrative storage measures –

A2 Automated delineation of rainfall driven events

Comparability of runoff coefficients requires essentially an automated detection of rainfall-runoff events in continuous time series to pool enough events into a statistically analyzable sample. The concept and interpretation of runoff coefficients (CR) on both event and annual time scales is old and dates back to Sherman (1932). Up to now CRs are frequently used as diagnostic variables to describe

Hydrol. Earth Syst. Sci. Discuss., doi:10.5194/hess-2016-109, 2016
Manuscript under review for journal Hydrol. Earth Syst. Sci.
Published: 9 March 2016

response properties and runoff generation (compare e.g., Pearce et al., 1986; Merz et al., 2006; Merz and Blöschl, 2009; Graeff et al., 2012; Capell et al., 2012, and many others). However, CRs are not defined consistently (e.g. total runoff over total precipitation vs. total quick flow over total precipitation) and the literature describes a range of different methods for the detection of the start and end of an event which are required for the separation of the slow flow component as illustrated by Blume et al. (2007). We extensively tested various approaches including baseflow separation and filtering techniques (e.g., Douglas and Peucker, 1973; Chapman, 1999; Perng et al., 2000; Eckhardt, 2005), penalty functions (Drabek, 2010), fuzzy logic (Seibert and Ehret, 2012), and the methods proposed by Merz and Blöschl (2009) and Norbiato et al. (2009). However, the results of these methods were usually unsatisfactory when applied to a range of different regimes of precipitation and stream flow. In the end we adapt and recombine different existing techniques and detect rainfall-runoff events based upon the following principles: First, we select *rainfall events* as subsequent periods of liquid rainfall (maximum up to 6 h of rain free period are tolerated) with at least 10 mm of daily rain depth (compare also Fig. 11). Given these periods, we identify the corresponding *discharge events* starting with the maximum flow rate. Between the latter and the beginning of rainfall we search for the first point in time where $dQ/dt > 0$ holds true for five subsequent time steps which we define as the start of the discharge event. Starting from the peak flow we next define the end of the discharge event using the constant-k method proposed by Blume et al. (2007). Due to missing convergence of this approach in 20 - 40 % of all cases we combine it with additional cut-off criteria (e.g. threshold exceedance, beginning of next rainfall event, and others). Missing convergence often results from varying rainfall intensities throughout the event. In our data set we observed that the occurrence of multiple peaks and troughs within a "single" event is more often the rule rather than the exception. Upon request, a program code for the automated detection of rainfall-runoff events in hourly time series which is written in R (R Development Core Team, 2015) can be obtained from the author.

– FIGURE 11: Automated detection of rainfall-runoff events –

A3 Linkage between site identifiers and gauge names

Table 6 relates the site identifiers we introduce in section 3 to the corresponding gauge and stream names.

– TABLE 6: Link table –

Acknowledgements. We gratefully acknowledge data provision by the Bavarian Environmental Agency (LfU) and the German (DWD) and Austrian weather services (ZAMG). Funding was partly provided by the LfU which is gratefully acknowledged as well. We also thank Hoshin Gupta for the inspiring discussion on the double and triple mass curve concepts a few years ago. We furthermore acknowledge support by Deutsche Forschungsgemeinschaft and Open Access Publishing Fund of Karlsruhe Institute of Technology.

Hydrol. Earth Syst. Sci. Discuss., doi:10.5194/hess-2016-109, 2016
Manuscript under review for journal Hydrol. Earth Syst. Sci.
Published: 9 March 2016

Hydrology and Earth System Sciences
Open Access
Discussions

References

Ali, G., Tetzlaff, D., Soulsby, C., McDonnell, J. J., and Capell, R.: A comparison of similarity indices for catchment classification using a cross-regional dataset, Adv. Water Resour., 40, 11–22, doi:10.1016/j.advwatres.2012.01.008, 2012.

Bergstroem, S.: Development and Application of a conceptual runoff model for Scandinavian catchment., Tech. rep., Swedish Meteorological and Hydrological Institute (SMHI), Report RHO 7, Norrkoping, 1976.

Berne, A., Uijlenhoet, R., and Troch, P. A.: Similarity analysis of subsurface flow response of hillslopes with complex geometry, Water Resour. Res., 41, 1–10, doi:10.1029/2004WR003629, 2005.

Best, D. and Roberts, D.: The Upper Tail Probabilities of Spearman's Rho, J. R. Stat. Soc. Ser. C, 24, 377–379, doi:10.2307/2347111, 1975.

Beven, K.: Changing ideas in hydrology - The case of physically-based models, J. Hydrol., 105, 157–172, doi:10.1016/0022-1694(89)90101-7, 1989.

Beven, K. and Germann, P.: Macropores and water flow in soils revisited, Water Resour. Res., 49, 3071–3092, doi:10.1002/wrcr.20156, 2013.

BGR: Bodenübersichtskarte von Deutschland 1:1,000,000 (BÜK1000), 1995.

BGR and SGD: Hydrogeological spatial structure of Germany (HYRAUM). Digital map data v3.2, 2015.

Binley, A. and Beven, K.: Vadose zone flow model uncertainty as conditioned on geophysical data, Ground Water, 41, 119–127, doi:10.1111/j.1745-6584.2003.tb02576.x, 2003.

Black, P. E.: Watershed Functions, J. Am. Water Resour. Assoc., 33, 1–11, doi:10.1111/j.1752-1688.1997.tb04077.x, 1997.

Blume, T., Zehe, E., and Bronstert, A.: Rainfall-runoff response, event-based runoff coefficients and hydrograph separation, Hydrol. Sci. J., 52, 843–862, doi:10.1623/hysj.52.5.843, 2007.

Brocca, L., Melone, F., Moramarco, T., and Singh, V. P.: Assimilation of Observed Soil Moisture Data in Storm Rainfall-Runoff Modeling, J. Hydrol. Eng., 14, 153–165, doi:10.1061/(ASCE)1084-0699(2009)14:2(153), 2009.

Brutsaert, W. and Nieber, J. L.: Regionalized drought flow hydrographs from a mature glaciated plateau, Water Resour. Res., 13, 637–643, doi:10.1029/WR013i003p00637, 1977.

Budyko, M. I.: The Heat Balance of the Earth's Surface, Sov. Geogr., 2, 3–13, doi:10.1080/00385417.1961.10770761, 1961.

Capell, R., Tetzlaff, D., Hartley, A. J., and Soulsby, C.: Linking metrics of hydrological function and transit times to landscape controls in a heterogeneous mesoscale catchment, Hydrol. Process., 26, 405–420, doi:10.1002/hyp.8139, 2012.

Carrillo, G., Troch, P. A., Sivapalan, M., Wagener, T., Harman, C., and Sawicz, K.: Catchment classification: Hydrological analysis of catchment behavior through process-based modeling along a climate gradient, Hydrol. Earth Syst. Sci., 15, 3411–3430, doi:10.5194/hess-15-3411-2011, 2011.

Chapman, T.: A comparison of algorithms for stream flow recession and baseflow separation, Hydrol. Process., 13, 701–714, doi:10.1002/(SICI)1099-1085(19990415)13:5<701::AID-HYP774>3.0.CO;2-2, 1999.

de Rooij, G. H.: Averaging hydraulic head, pressure head, and gravitational head in subsurface hydrology, and implications for averaged fluxes, and hydraulic conductivity, Hydrol. Earth Syst. Sci., 13, 1123–1132, doi:10.5194/hess-13-1123-2009, 2009.

Hydrology and Earth System Sciences
Open Access
Discussions

de Rooij, G. H.: Averaged water potentials in soil water and groundwater, and their connection to menisci in soil pores, field-scale flow phenomena, and simple groundwater flows, Hydrol.Earth Syst.Sci., 15, 1601–1614, doi:10.5194/hess-15-1601-2011, 2011.

Dooge, J. C. I.: Looking for hydrological laws, Water Resour. Res., 22, 46S–58S, 1986.

Douglas, D. H. and Peucker, T. K.: Algorithms for the Reduction of the Number of Points Required To Represent a Digitized Line or Its Caricature, Cartogr. Int. J. Geogr. Inf. Geovisualization, 10, 112–122, doi:10.3138/FM57-6770-U75U-7727, 1973.

Drabek, U.: Anwendungsbezogene Aspekte der operationellen Durchflussvorhersage, Ph.D. thesis, Institut für Wasserbau und Ingenieurhydrologie, Technische Universität Wien, Wien, 2010.

Duan, Q., Schaake, J., Andréassian, V., Franks, S., Goteti, G., Gupta, H., Gusev, Y., Habets, F., Hall, A., Hay, L., Hogue, T., Huang, M., Leavesley, G., Liang, X., Nasonova, O., Noilhan, J., Oudin, L., Sorooshian, S., Wagener, T., and Wood, E.: Model Parameter Estimation Experiment (MOPEX): An overview of science strategy and major results from the second and third workshops, J. Hydrol., 320, 3–17, doi:10.1016/j.jhydrol.2005.07.031, 2006.

Dunne, T. and Black, R. D.: An experimental investigation of runoff production in permeable soils, Water Resour. Res., 6, 478–490, doi:10.1029/WR006i002p00478, 1970.

Duscher, K., Günther, A., Richts, A., Clos, P., Philipp, U., and Struckmeier, W.: The GIS layers of the 'International Hydrogeological Map of Europe 1:1,500,000' in a vector format, Hydrogeol. J., 23, 1867–1875, 2015.

Eckhardt, K.: How to construct recursive digital filters for baseflow separation, Hydrol. Process., 19, 507–515, doi:10.1002/hyp.5675, 2005.

Ehret, U., Götzinger, J., Bardossy, A., and Pegram, G. G.: Radar-based flood forecasting in small catchments, exemplified by the Goldersbach catchment, Germany, Int. J. River Basin Manag., 6, 323–329, doi:10.1080/15715124.2008.9635359, 2008.

Fenicia, F., Savenije, H. H. G., Matgen, P., and Pfister, L.: Is the groundwater reservoir linear? Learning from data in hydrological modelling, Hydrol. Earth Syst. Sci., 10, 139–150, 2006.

Fiener, P. and Auerswald, K.: Spatial Variability of rainfall on a sub-kilometer scale, Earth Surf. Process. Landforms, 34, 848–859, 2009.

Fiener, P., Seibert, S. P., and Auerswald, K.: A compilation and meta-analysis of rainfall simulation data on arable soils, J. Hydrol., 409, 395–406, doi:10.1016/j.jhydrol.2011.08.034, 2011.

Fiener, P., Auerswald, K., Winter, F., and Disse, M.: Statistical analysis and modelling of surface runoff from arable fields in central Europe, Hydrol. Earth Syst. Sci., 17, 4121–4132, doi:10.5194/hess-17-4121-2013, 2013.

Gassmann, M., Stamm, C., Olsson, O., Lange, J., Kümmerer, K., and Weiler, M.: Model-based estimation of pesticides and transformation products and their export pathways in a headwater catchment, Hydrol. Earth Syst. Sci., 17, 5213–5228, doi:10.5194/hess-17-5213-2013, 2013.

Goodrich, D. C., Faurès, J.-M., Woolhiser, D. a., Lane, L. J., and Sorooshian, S.: Measurement and analysis of small-scale convective storm rainfall variability, J. Hydrol., 173, 283–308, doi:10.1016/0022-1694(95)02703-R, 1995.

Graeff, T., Zehe, E., Reusser, D., Lück, E., Schröder, B., Wenk, G., John, H., and Bronstert, A.: Process identification through rejection of model structures in a mid-mountainous rural catchment: observations of rainfall-runoff response, geophysical conditions and model inter-comparison, Hydrol. Process., 23, 702–718, doi:10.1002/hyp.7171, 2009.

Graeff, T., Zehe, E., Blume, T., Francke, T., and Schröder, B.: Predicting event response in a nested catchment with generalized linear models and a distributed watershed model, Hydrol. Process., 26, 3749–3769, doi:10.1002/hyp.8463, 2012.

He, Y., Bárdossy, a., and Zehe, E.: A catchment classification scheme using local variance reduction method, J. Hydrol., 411, 140–154, doi:10.1016/j.jhydrol.2011.09.042, 2011.

Heggen, R. J.: Normalized Antecedent Precipitation Index, J. Hydrol. Eng., 6, 377–381, doi:10.1061/(ASCE)1084-0699(2001)6:5(377), 2001.

Hellebrand, H., Van Den Bos, R., Hoffmann, L., Juilleret, J., and Pfister, L.: The potential of winter stormflow coefficients for hydrological regionalization purposes in poorly gauged basins of the middle Rhine region, Hydrol. Sci. J., 53, 773–788, doi:10.1623/hysj.53.4.773, 2008.

Hohmann, C.: Threshold behaviour in hydrological systems as (human) geo-ecosystems: manifestations, controls, implications by E. Zehe and M. Sivapalan, Hydrol. Earth Syst. Sci., 13, 1–8, doi:10.5194/hess-13-1273-2009, 2014.

Horton, R. E.: Analysis of runoff-plot experiments with varying infiltration-capacity, Trans. Am. Geophys. Union, 20, 693, doi:10.1029/TR020i004p00693, 1939.

Hundecha, Y. and Bárdossy, A.: Modeling of the effect of land use changes on the runoff generation of a river basin through parameter regionalization of a watershed model, J. Hydrol., 292, 281–295, doi:10.1016/j.jhydrol.2004.01.002, 2004.

Kelleher, C., Wagener, T., and McGlynn, B.: Model-based analysis of the influence of catchment properties on hydrologic partitioning across five mountain headwater sub-catchments, Water Resour. Res., 51, 2–31, doi:10.1002/acr.22212, 2015.

Kenney, B. C.: Beware of spurious self-correlations!, Water Resour. Res., 18, 1041–1048, doi:10.1029/WR018i004p01041, 1982.

Kirchner, J. W.: Catchments as simple dynamical systems: Catchment characterization, rainfall-runoff modeling, and doing hydrology backward, Water Resour. Res., 45, 1–34, doi:10.1029/2008WR006912, 2009.

Klaus, J., Wetzel, C. E., Martínez-Carreras, N., Ector, L., and Pfister, L.: A tracer to bridge the scales: on the value of diatoms for tracing fast flow path connectivity from headwaters to meso-scale catchments, Hydrol. Process., 29, 5275–5289, doi:10.1002/hyp.10628, 2015.

Kleidon, A.: How does the Earth system generate and maintain thermodynamic disequilibrium and what does it imply for the future of the planet?, Philos. Trans. A. Math. Phys. Eng. Sci., 370, 1012–40, doi:10.1098/rsta.2011.0316, 2012.

Kneis, D. and Heistermann, M.: Bewertung der Güte einer Radar-basierten Niederschlagsschätzung am Beispiel eines kleinen Einzugsgebiets, Hydrol. und Wasserbewirtschaftung, 53, 160–171, 2009.

Laurenson, E. M.: A catchment storage model for runoff routing, J. Hydrol., 2, 141–163, doi:10.1016/0022-1694(64)90025-3, 1964.

Lehmann, P., Hinz, C., McGrath, G., Tromp-van Meerveld, H.-J., and McDonnell, J. J.: Rainfall threshold for hillslope outflow: an emergent property of flow pathway connectivity, Hydrol. Earth Syst. Sci. Discuss., 3, 2923–2961, doi:10.5194/hessd-3-2923-2006, 2006.

Lindsay J.B.: The Whitebox Geospatial Analysis Tools project and open-access GIS, in: Proc. GIS Res. UK 22nd Annu. Conf., p. 8, doi:10.13140/RG.2.1.1010.8962, 2014.

Ludwig, K. and Bremicker, M.: The Water Balance Model LARSIM, Tech. Rep. 22, Institut für Hydrologie der Universität Freiburg i.Br., 2006.

Maidment, D.: Handbook of Hydrology., McGraw-Hill Education, New York, NY, 1993.

Martínez-Carreras, N., Krein, A., Gallart, F., Iffly, J. F., Pfister, L., Hoffmann, L., and Owens, P. N.: Assessment of different colour parameters for discriminating potential suspended sediment sources and provenance: A multi-scale study in Luxembourg, Geomorphology, 118, 118–129, doi:10.1016/j.geomorph.2009.12.013, 2010.

Martínez-Carreras, N., Wetzel, C. E., Frentress, J., Ector, L., McDonnell, J. J., Hoffmann, L., and Pfister, L.: Hydrological connectivity inferred from diatom transport through the riparian-stream system, Hydrol. Earth Syst. Sci., 19, 3133–3151, doi:10.5194/hess-19-3133-2015, 2015.

McGuire, K. J., McDonnell, J. J., Weiler, M., Kendall, C., McGlynn, B. L., Welker, J. M., and Seibert, J.: The role of topography on catchment-scale water residence time, Water Resour. Res., 41, 1–14, doi:10.1029/2004WR003657, 2005.

McNamara, J. P., Tetzlaff, D., Bishop, K., Soulsby, C., Seyfried, M., Peters, N. E., Aulenbach, B. T., and Hooper, R.: Storage as a Metric of Catchment Comparison, Hydrol. Process., 25, 3364–3371, doi:10.1002/hyp.8113, 2011.

Menzel, A., Jakobi, G., Ahas, R., Scheifinger, H., and Estrella, N.: Variations of the climatological growing season (1951–2000) in Germany compared with other countries, Int. J. Climatol., 23, 793–812, doi:10.1002/joc.915, 2003.

Merz, R. and Blöschl, G.: A process typology of regional floods, Water Resour. Res., 39, n/a–n/a, doi:10.1029/2002WR001952, 2003.

Merz, R. and Blöschl, G.: A regional analysis of event runoff coefficients with respect to climate and catchment characteristics in Austria, Water Resour. Res., 45, 1–19, doi:10.1029/2008WR007163, 2009.

Merz, R., Blöschl, G., and Parajka, J.: Spatio-temporal variability of event runoff coefficients, J. Hydrol., 331, 591–604, doi:10.1016/j.jhydrol.2006.06.008, 2006.

Niehoff, D., Fritsch, U., and Bronstert, A.: Land-use impacts on storm-runoff generation: scenarios of land-use change and simulation of hydrological response in a meso-scale catchment in SW-Germany, J. Hydrol., 267, 80–93, doi:10.1016/S0022-1694(02)00142-7, 2002.

Nippgen, F., McGlynn, B. L., and Emanuel, R. E.: The spatial and temporal evolution of contributing areas, Water Resour. Res., 51, 4550–4573, doi:10.1002/2014WR016719, 2015.

Norbiato, D., Borga, M., Merz, R., Blöschl, G., and Carton, A.: Controls on event runoff coefficients in the eastern Italian Alps, J. Hydrol., 375, 312–325, doi:10.1016/j.jhydrol.2009.06.044, 2009.

Palm, J., van Schaik, N. L. M. B., and Schröder, B.: Modelling distribution patterns of anecic, epigeic and endogeic earthworms at catchment-scale in agro-ecosystems, Pedobiologia (Jena)., 56, 23–31, doi:10.1016/j.pedobi.2012.08.007, 2013.

Pearce, a. J., Stewart, M. K., and Sklash, M. G.: Storm Runoff Generation in Humid Headwater Catchments: 1. Where Does the Water Come From?, Water Resour. Res., 22, 1263, doi:10.1029/WR022i008p01263, 1986.

Pearson, P. K.: Mathematical contributions to the theory of evolution. On a form of spurious correlation which may arise when indices are used in the measurments of organs., Proc. R. Soc. London, 60, 489–498, 1897.

Perng, C.-S., Wang, H., Zhang, S., and Parker, D.: Landmarks: a new model for similarity-based pattern querying in time series databases, Proc. 16th Int. Conf. Data Eng. (Cat. No.00CB37073), pp. 33–42, doi:10.1109/ICDE.2000.839385, 2000.

Peschke, G.: Zur Bildung und Berechnung von Regenabfluss, Wissenschaftliche Zeitschrift der Tech. Univ. Dresden, 34, 195–200, 1985.

Peschke, G., Etzenberg, C., Müller, G., Töpfer, J., and Zimmermann, S.: Das wissensbasierte System FLAB - ein Instrument zur rechnergestützten Bestimmung von Landschaftseinheiten mit gleicher Abflussbilung, 10, Internationales Hochschulinstitut Zittau, 1999.

Pfister, L., Iffly, J. F., and Hoffmann, L.: Use of regionalized stormflow coefficients with a view to hydroclimatological hazard mapping, Hydrol. Sci. Journal-Journal Des Sci. Hydrol., 47, 479–491, doi:10.1080/02626660209492948, 2002.

Pfister, L., Drogue, G., El Idrissi, a., Humbert, J., Iffly, J., Matgen, P., and Hoffmann, L.: Predicting peak discharge through empirical relationships between rainfall, groundwater level and basin humidity in the Alzette river basin (grand-duchy of Luxembourg), 2003.

R Development Core Team: R: A Language and Environment for Statistical Computing., doi:10.1007/978-3-540-74686-7, 2015.

Refsgaard, J. C.: Validation and intercomparision of different updating procedure for real time flood forecasting, Nord. Hydrol., 28, 65–84, 1997.

Reggiani, P., Sivapalan, M., and Hassanizadeh, S. M.: Conservation equations governing hillslope responses: Exploring the physical basis of water balance, Water Resour. Res., 36, 1845, doi:10.1029/2000WR900066, 2000.

Rodríguez-Iturbe, I. and Valdés, J. B.: The geomorphologic structure of hydrologic response, Water Resour. Res., 15, 1409, doi:10.1029/WR015i006p01409, 1979.

Ruiz-Villanueva, V., Borga, M., Zoccatelli, D., Marchi, L., Gaume, E., and Ehret, U.: Extreme flood response to short-duration convective rainfall in South-West Germany, Hydrol. Earth Syst. Sci., 16, 1543–1559, doi:10.5194/hess-16-1543-2012, 2012.

Saghafian, B., Julien, P. Y., and Ogden, F. L.: Similarity in catchment response: 1. Stationary rainstorms, Water Resour. Res., 31, 1533–1541, doi:10.1029/95WR00518, 1995.

Sawicz, K., Wagener, T., Sivapalan, M., Troch, P. a., and Carrillo, G.: Catchment classification: Empirical analysis of hydrologic similarity based on catchment function in the eastern USA, Hydrol. Earth Syst. Sci., 15, 2895–2911, doi:10.5194/hess-15-2895-2011, 2011.

Sayama, T., McDonnell, J. J., Dhakal, A., and Sullivan, K.: How much water can a watershed store?, Hydrol. Process., 25, 3899–3908, doi:10.1002/hyp.8288, 2011.

Schaake, J., Duan, Q., Smith, M., and Koren, V.: Criteria to select basins for hydrologic model development and testing, 15th Conference on Hydrology (P1.8), AMS, January 9-14. Long Beach, CA, 2000.

Schaap, M. G., Leij, F. J., and van Genuchten, M. T.: Rosetta: a computer program for estimating soil hydraulic parameters with hierarchical pedotransfer functions, J. Hydrol., 251, 163–176, doi:http://dx.doi.org/10.1016/S0022-1694(01)00466-8, 2001.

Schaefli, B., Harman, C. J., Sivapalan, M., and Schymanski, S. J.: HESS Opinions: Hydrologic predictions in a changing environment: behavioral modeling, Hydrol. Earth Syst. Sci., 15, 635–646, doi:10.5194/hess-15-635-2011, 2011.

Schmocker-Fackel, P., Naef, F., and Scherrer, S.: Identifying runoff processes on the plot and catchment scale, Hydrol. Earth Syst. Sci., 11, 891–906, doi:10.5194/hessd-3-2063-2006, 2007.

Seibert, S. P. and Ehret, U.: Quantification and visualisation of timing and amplitude uncertainties in the simulatio and forecast of discharge time series, Submitt. to Hydrol. Earth Syst. Sci., NA, NA.

Seibert, S. P. and Ehret, U.: Detection of flood events in hydrological discharge time series (EGU2012-5924), in: Geophys. Res. Abstr., vol. 14, 2012.

Seibert, S. P., Skublics, D., and Ehret, U.: The potential of coordinated reservoir operation for flood mitigation in large basins - A case study on the Bavarian Danube using coupled hydrological-hydrodynamic models, J. Hydrol., 517, 1128–1144, doi:10.1016/j.jhydrol.2014.06.048, 2014.

Shaw, S. B. and Riha, S. J.: Examining individual recession events instead of a data cloud: Using a modified interpretation of dQ/dt–Q streamflow recession in glaciated watersheds to better inform models of low flow, J. Hydrol., 434–435, 46–54, doi:http://dx.doi.org/10.1016/j.jhydrol.2012.02.034, 2012.

Sherman, L. K.: Streamflow from rainfall by the unit graph method, Eng. News Rec., 108, 501–505, 1932.

Soulsby, C., Tetzlaff, D., and Hrachowitz, M.: Tracers and transit times: windows for viewing catchment storage?, Hydrol. Process., 23, 3503–3507, doi:10.1002/hyp, 2009.

Spence, C.: On the relation between dynamic storage and runoff: A discussion on thresholds, efficiency, and function, Water Resour. Res., 43, 1–11, doi:10.1029/2006WR005645, 2007.

Struthers, I. and Sivapalan, M.: A conceptual investigation of process controls upon flood frequency: role of thresholds, Hydrol. Earth Syst. Sci., 11, 1405–1416, doi:10.5194/hess-11-1405-2007, 2007.

Struthers, I., Hinz, C., and Sivapalan, M.: Conceptual examination of climate–soil controls upon rainfall partitioning in an open-fractured soil II: Response to a population of storms, Adv. Water Resour., 30, 518–527, doi:10.1016/j.advwatres.2006.04.005, 2007a.

Struthers, I., Sivapalan, M., and Hinz, C.: Conceptual examination of climate–soil controls upon rainfall partitioning in an open-fractured soil: I. Single storm response, Adv. Water Resour., 30, 505–517, doi:10.1016/j.advwatres.2006.04.006, 2007b.

Tetzlaff, D., McNamara, J. P., and Carey, S. K.: Measurements and modelling of storage dynamics across scales, Hydrol. Process., 25, 3831–3835, doi:10.1002/hyp.8396, 2011.

Toloczyki, M., Trurnit, P., Voges, A., and Wittekindt, H.: Geological Map of Germany 1:1,000,000 (GK1000), 2006.

Troch, P. A., Paniconi, C., and Emiel van Loon, E.: Hillslope-storage Boussinesq model for subsurface flow and variable source areas along complex hillslopes: 1. Formulation and characteristic response, Water Resour. Res., 39, 1316, doi:10.1029/2002wr001728, 2003.

Tromp-van Meerveld, H. J. and McDonnell, J. J.: Threshold relations in subsurface stormflow: 1. A 147-storm analysis of the Panola hillslope, Water Resour. Res., 42, n/a–n/a, doi:10.1029/2004WR003778, 2006.

US Department of Commerce: NOAA Technical Memorandum NWS-Hydro-14. National Weather Service River Forcast System Forecast Procedures, Tech. rep., Washington, D.C., 1972.

Van Schaik, L., Palm, J., Klaus, J., Zehe, E., and Schröder, B.: Linking spatial earthworm distribution to macropore numbers and hydrological effectiveness, Ecohydrology, 7, 401–408, doi:10.1002/eco.1358, 2014.

Wagener, T., Sivapalan, M., Troch, P., and Woods, R.: Catchment Classification and Hydrologic Similarity, Geogr. Compass, 1, 1–31, doi:10.1111/j.1749-8198.2007.00039.x, 2007.

Wienhöfer, J. and Zehe, E.: Predicting subsurface stormflow response of a forested hillslope – the role of connected flow paths, Hydrol. Earth Syst. Sci., 18, 121–138, doi:10.5194/hess-18-121-2014, 2014.

Wienhöfer, J., Germer, K., Lindenmaier, F., Färber, a., and Zehe, E.: Applied tracers for the observation of subsurface stormflow at the hillslope scale, Hydrol. Earth Syst. Sci. Discuss., 6, 2961–3006, doi:10.5194/hessd-6-2961-2009, 2009.

Woods, R.: The relative roles of climate, soil, vegetation and topography in determining seasonal and long-term catchment dynamics, Adv. Water Resour., 26, 295–309, doi:10.1016/S0309-1708(02)00164-1, 2003.

Woods, R. A.: Analytical model of seasonal climate impacts on snow hydrology: Continuous snowpacks, Adv. Water Resour., 32, 1465–1481, doi:10.1016/j.advwatres.2009.06.011, 2009.

Zehe, E. and Blöschl, G.: Predictability of hydrologic response at the plot and catchment scales: Role of initial conditions, Water Resour. Res., 40, 1–21, doi:10.1029/2003WR002869, 2004.

Zehe, E., Becker, R., Bárdossy, A., and Plate, E.: Uncertainty of simulated catchment runoff response in the presence of threshold processes: Role of initial soil moisture and precipitation, J. Hydrol., 315, 183–202, doi:10.1016/j.jhydrol.2005.03.038, 2005.

Zehe, E., Lee, H., and Sivapalan, M.: Dynamical process upscaling for deriving catchment scale state variables and constitutive relations for meso-scale process models, Hydrol. Earth Syst. Sci. Discuss., 3, 1629–1665, doi:10.5194/hessd-3-1629-2006, 2006.

Zehe, E., Elsenbeer, H., Lindenmaier, F., Schulz, K., and Blöschl, G.: Patterns of predictability in hydrological threshold systems, Water Resour. Res., 43, 1–12, doi:10.1029/2006WR005589, 2007.

Zehe, E., Graeff, T., Morgner, M., Bauer, A., and Bronstert, A.: Plot and field scale soil moisture dynamics and subsurface wetness control on runoff generation in a headwater in the Ore Mountains, Hydrol. Earth Syst. Sci., 14, 873–889, doi:10.5194/hess-14-873-2010, 2010.

Zehe, E., Ehret, U., Blume, T., Kleidon, A., Scherer, U., and Westhoff, M.: A thermodynamic approach to link self-organization, preferential flow and rainfall–runoff behaviour, Hydrol. Earth Syst. Sci., 17, 4297–4322, doi:10.5194/hess-17-4297-2013, 2013.

Zehe, E., Ehret, U., Pfister, L., Blume, T., Schröder, B., Westhoff, M., Jackisch, C., Schymanski, S. J., Weiler, M., Schulz, K., Allroggen, N., Tronicke, J., van Schaik, L., Dietrich, P., Scherer, U., Eccard, J., Wulfmeyer, V., and Kleidon, A.: HESS Opinions: From response units to functional units: a thermodynamic reinterpretation of the HRU concept to link spatial organization and functioning of intermediate scale catchments, Hydrol. Earth Syst. Sci., 18, 4635–4655, doi:10.5194/hess-18-4635-2014, 2014.

Hydrol. Earth Syst. Sci. Discuss., doi:10.5194/hess-2016-109, 2016
Manuscript under review for journal Hydrol. Earth Syst. Sci.
Published: 9 March 2016

Hydrology and Earth System Sciences
Open Access
Discussions

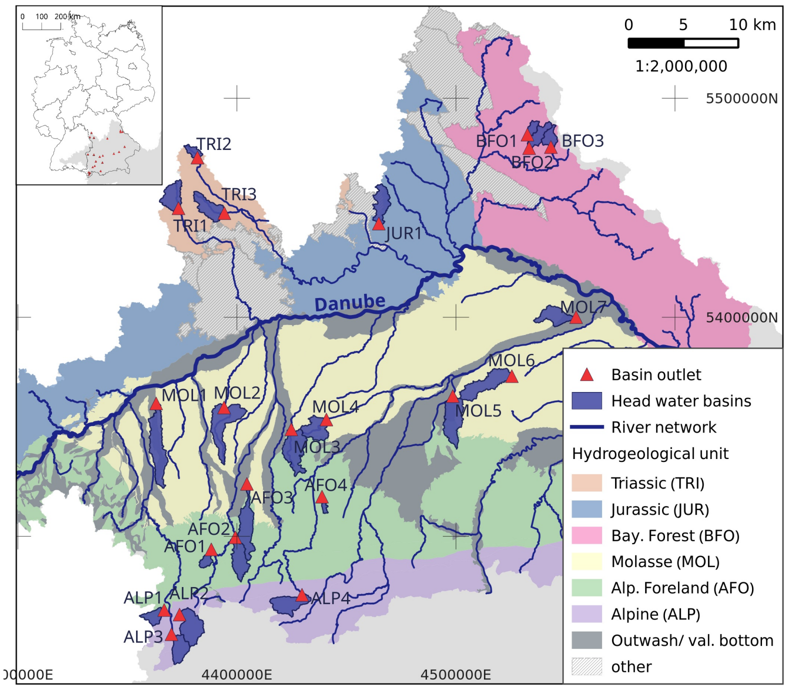

Figure 1. Upper Danube catchment in southern Germany with selected head water basins (blue polygons), corresponding gauges (red triangles) and major river network (blue lines). The site identifiers (IDs) refer to the corresponding (hydro)geological unit (color coded map in the background, adapted from BGR and SGD (2015)) and a single Arabic numeral. Moving from the North-West to the South we differentiate TRI (Triassic), JUR (Jurasic), BFO (Bavarian Forest), MOL (Faulted Molasse), AFO (Alpine Foreland) and ALP (Alpine). Appendix A3 provides links between the site IDs and the real gauge names. The inset in the upper left corner shows Germany's federal state boundaries, the individual head water outlets and the basin of the Danube (grey area). The grid coordinates refer to the Gauss-Kruger zone 4 projection (CRS identifier EPSG:31468).

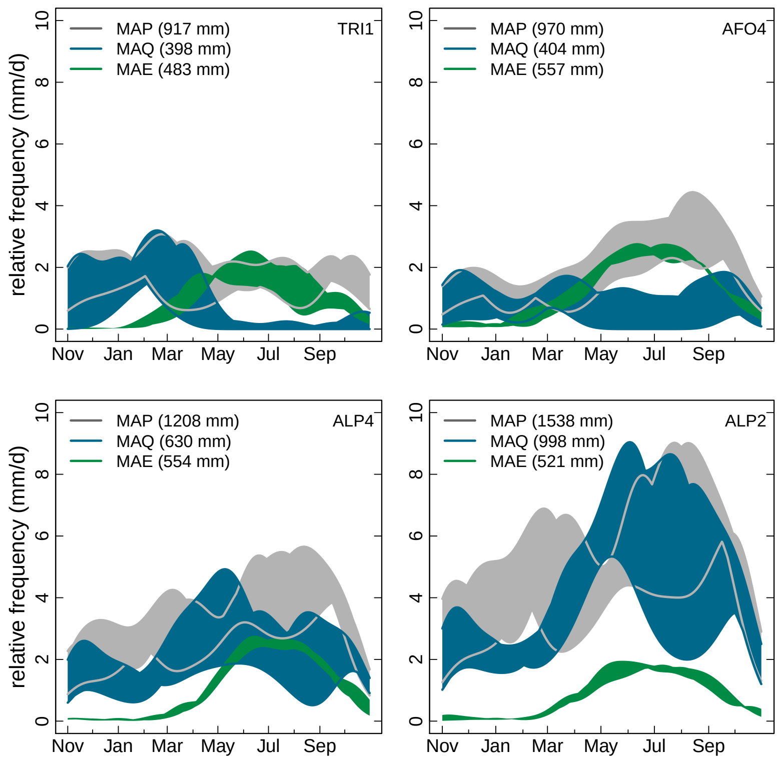

Figure 2. Kernel density estimates (regime curves) of observed areal precipitation (grey), discharge (blue) and calculated areal mean evapotranspiration (Penman-Monteith) (green) of four selected head water catchments. The width of the individual bands illustrates the inter-annual variation during the four year lasting period. In all cases identical kernels and bandwidths are used for variables of the same type. MAP, MAQ and MAE provide information on the four year mean annual average for P, Q and E respectively.

Hydrol. Earth Syst. Sci. Discuss., doi:10.5194/hess-2016-109, 2016
Manuscript under review for journal Hydrol. Earth Syst. Sci.
Published: 9 March 2016

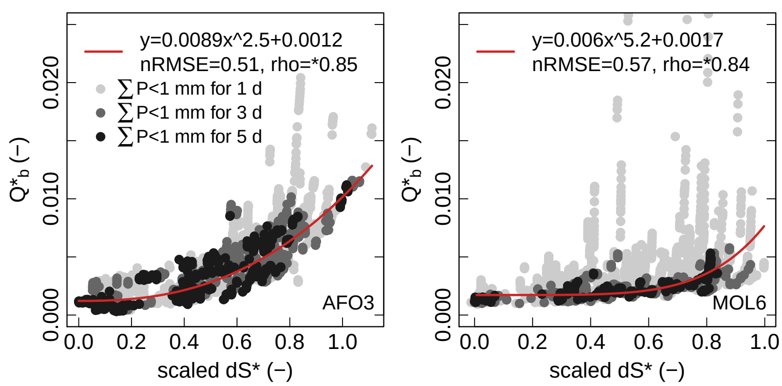

Figure 3. Normalized empirical storage-baseflow relationship for the catchments AFO3 (left) and MOL6 (right). dS^* and Q_b^* are calculated according to Eq. (1 and 4), respectively. The power law functions (red lines) are fitted to stream flow values where the last input in precipitation > 0.1 mm was $\geq$ 5 d ago (statistics in the top). The quality of each relation is judged using the root-mean-square-error normalized to the standard deviation of the sample (nRMSE) and Spearman's rank coefficient of correlation (rho). Note: Fitting the model to the data required a re-scaling of dS^* to the range $[0..\infty]$ to prevent root extraction from negative values.

Hydrol. Earth Syst. Sci. Discuss., doi:10.5194/hess-2016-109, 2016
Manuscript under review for journal Hydrol. Earth Syst. Sci.
Published: 9 March 2016

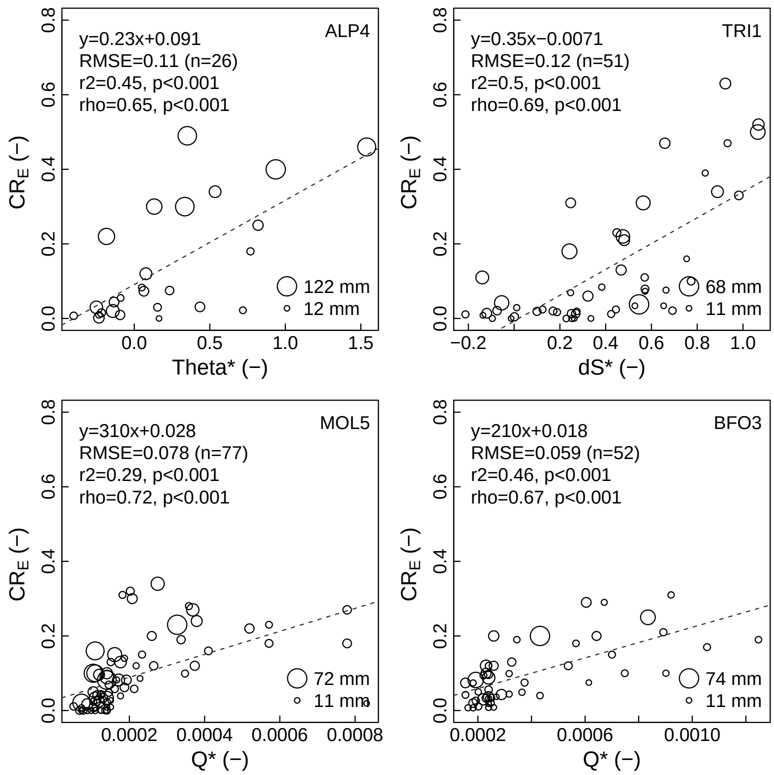

Figure 4. Event runoff coefficients (CR_E) plotted against the normalized storage measures θ^*, dS^* or Q^* for the sites ALP4, TRI1, MOL5 and BFO3. The point sizes are scaled according to the corresponding rain depth. Statistical information is provided in terms of a regression (dotted line), its equation, the sample size (n), the root-mean-squared-error (RMSE), Pearsons' coefficient of determination (r^2), Spearmans' rank coefficient of correlation (rho) and corresponding p-values (p).

Hydrol. Earth Syst. Sci. Discuss., doi:10.5194/hess-2016-109, 2016
Manuscript under review for journal Hydrol. Earth Syst. Sci.
Published: 9 March 2016

Hydrology and Earth System Sciences
Discussions

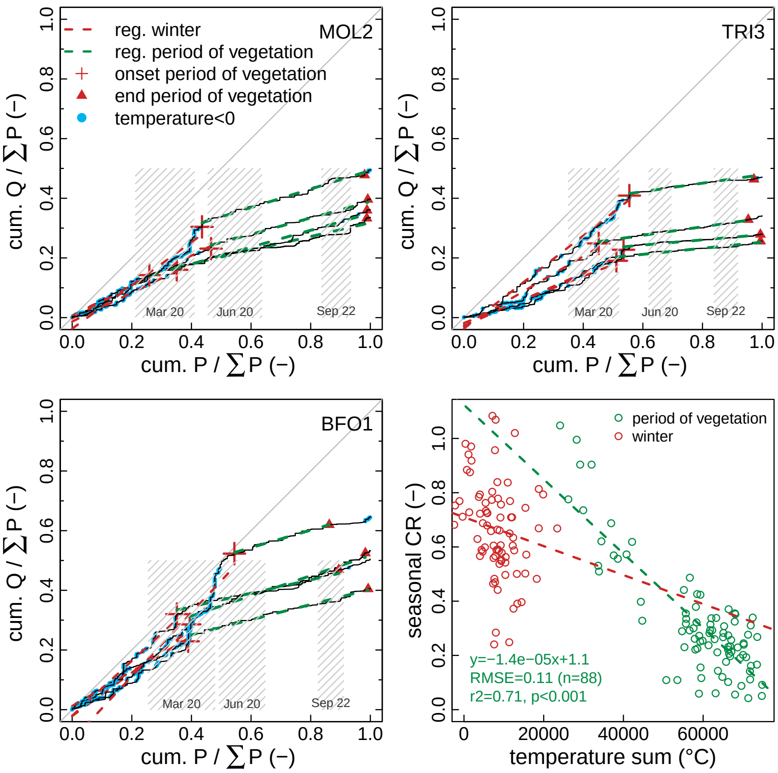

Figure 5. Normalized double mass curves (nDMC) for the catchments MOL2 (*top left*), TRI3 (*top right*) and BFO1 (*bottom left*) for the hydrological years 1999-2003. Onset and end of the period of vegetation are determined using a temperature index model. Regression lines are fitted to both periods (dotted lines in red/ green), their slopes are interpreted as seasonal runoff coefficients. Periods with temperatures < 0 °C are highlight in blue. Gregorian definitions for the start of spring (Mar 20th), start of summer (Jun 20th) and start of fall (Sep 22th) (hatched polygons) are added to the $cum.P/\sum P$ plane to highlight their differences to temperature based estimates on the onset and end of the period of vegetation. Statistical properties of all nDMCs are summarized in Table 5. The *bottom right panel* shows seasonal hourly temperature sums (calculated for each hydrological year starting from Nov 1st) and corresponding seasonal runoff coefficients for all sites (n=22) and years (n=4). The dotted lines are regressions. Statistical information on the summer model is plotted in green. During winter there was no significant statistical relation available (r^2=0.04, p=0.062).

Hydrol. Earth Syst. Sci. Discuss., doi:10.5194/hess-2016-109, 2016
Manuscript under review for journal Hydrol. Earth Syst. Sci.
Published: 9 March 2016

Hydrology and Earth System Sciences
Discussions

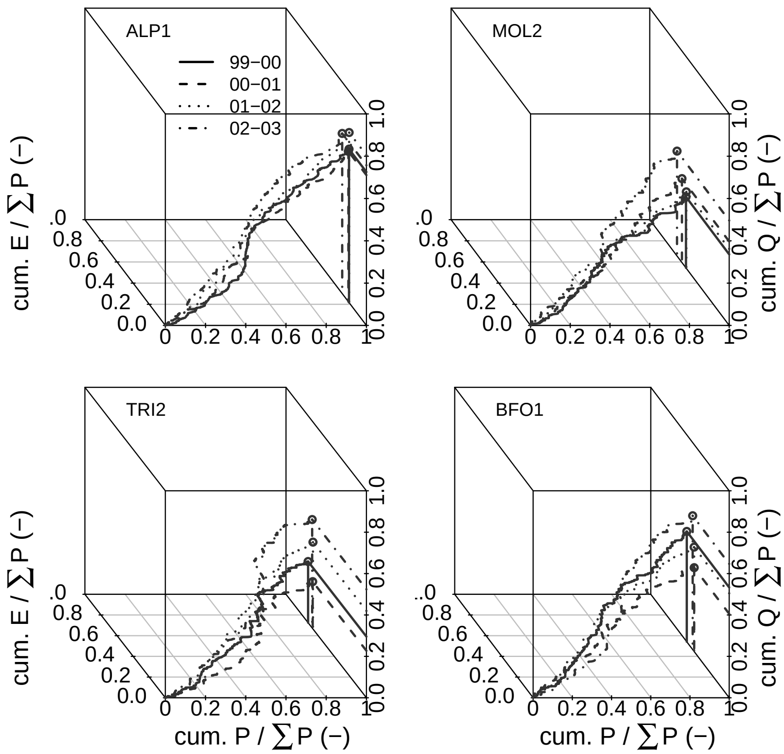

Figure 6. Normalized triple mass curves (nTMCs) from the catchments ALP1, MOL2, TRI2 and BFO1. Each plot contains data from four different hydrological years ('99-'00, '00-'01, '01-'02 and '02-'03) which are coded using different line styles. In the *upper row* (sites ALP1 and MOL2) the inter-annual variations in $cum.Q/\sum P$ are rather identical to the inter-annual variations in $cum.E/\sum P$. At TRI2 and BFO1 (*lower row*), the inter-annual variations in $cum.Q/\sum P$ are much larger than the inter-annual variations in $cum.E/\sum P$. Corresponding statistics of the normalized double and triple mass curves are summarized in Table 5.

Hydrology and Earth System Sciences
Open Access
Discussions

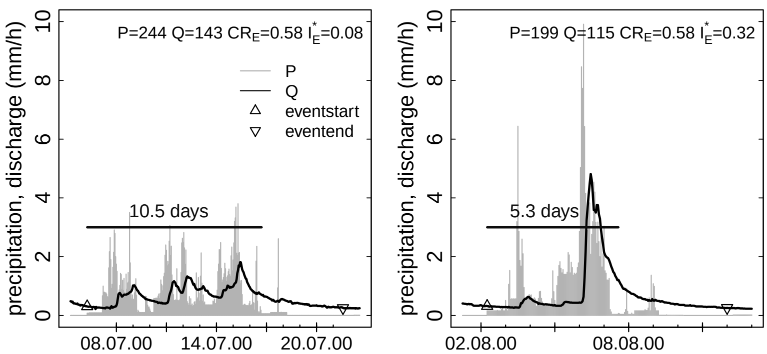

Figure 7. Two storm events from the alpine catchment ALP2 with almost similar total amounts of precipitation (P) and discharge (Q), identical runoff coefficient (CR_E), but with different duration and thus, intensities. The latter is reflected in different I_E^* (Eq. 7) which corresponds to the normalized maximum temporal change in intensity. In the first case (*left panel*) we expect that capacity controlled processes to dominate the runoff generation. In the second case (*right panel*) we assume that the steep rising limb and the high peak discharge are caused by intensity controlled runoff formation processes.

Hydrology and Earth System Sciences Discussions
Open Access

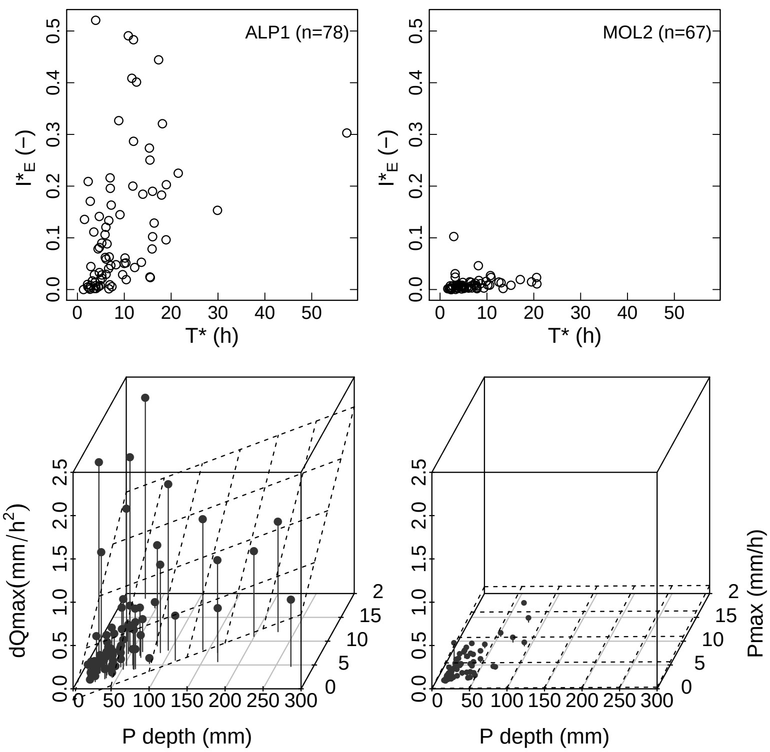

Figure 8. Diagnostics for the detection of intensity controlled conditions. The panels in the *upper row* show scatterplots of the normalized event duration T_E^* (Eq. 6) which is plotted against the normalized temporal intensity changes (I_E^*) (Eq. 7). The *lower row* shows corresponding three-dimensional scatterplots with event rain depth, maximum observed rain intensity and the maximum of the temporal derivative of observed discharge ($dI_{Q,max}$) are plotted on the x, y and z-axis respectively. The inclined plane (dotted) represents the plane of a multiple linear regression. The left column shows a conclusive case (site ALP1) where the frequent occurrence of intensity controlled runoff formation processes is likely. The right column shows inconclusive results from the site MOL2.

Hydrol. Earth Syst. Sci. Discuss., doi:10.5194/hess-2016-109, 2016
Manuscript under review for journal Hydrol. Earth Syst. Sci.
Published: 9 March 2016

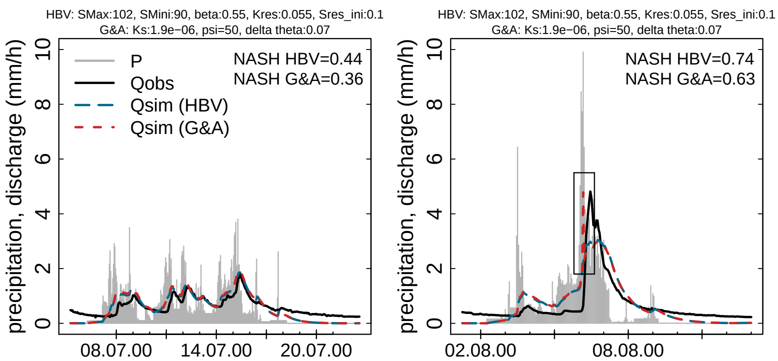

Figure 9. Simulated storm hydrographs from a capacity controlled event (*left*) and a (partly) intensity controlled event (*right*). Simulations use a HBV type betastore (red line) and a Green and Ampt (G&A) approach (blue line). Both concepts are combined with a linear reservoir. For the HBV type we optimize maximum storage depth ($SMax$), beta parameter ($beta$) and reservoir constant ($kres$) in an event based mode using a simulated annealing algorithm (initial fillings of the betastore $SMini$ and of the linear reservoir $Sres, ini$ are insensitive to the peak flow simulation accuracy). G&A is parametrized based upon a Rosetta (Schaap et al., 2001) estimate of Ks and a literature value for the suction head (psi) at the wetting front (Maidment, 1993). The parameters of the linear reservoir ($SMax$ and $kres$) are adopted from the HBV optimization. As (statistical) reference for the model performance we provide the Nash-Sutcliffe-Efficiency (NASH) criterion. Statistics of the rainfall-runoff events are provided in Fig. 7.

Hydrol. Earth Syst. Sci. Discuss., doi:10.5194/hess-2016-109, 2016
Manuscript under review for journal Hydrol. Earth Syst. Sci.
Published: 9 March 2016

Hydrology and Earth System Sciences
Open Access
Discussions

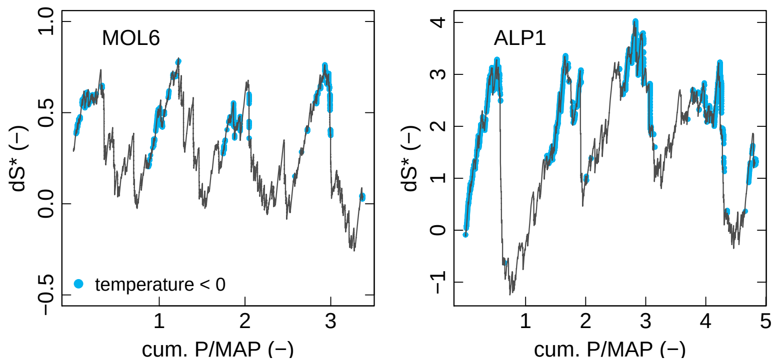

Figure 10. Coherent normalization of integrative storage measures. The plots show examples from the sites MOL6 and ALP1 for the same four year period (11/1999-10/2003). Re-scaled and normalized dynamic storage dS^* (Eq. 1) is plotted on the ordinate, the abscissa shows cumulated precipitation divided by the long term mean annual precipitation (MAP). Please note the differences between the two sites in the scaling of the axes.

Hydrol. Earth Syst. Sci. Discuss., doi:10.5194/hess-2016-109, 2016
Manuscript under review for journal Hydrol. Earth Syst. Sci.
Published: 9 March 2016

Hydrology and Earth System Sciences
Open Access
Discussions

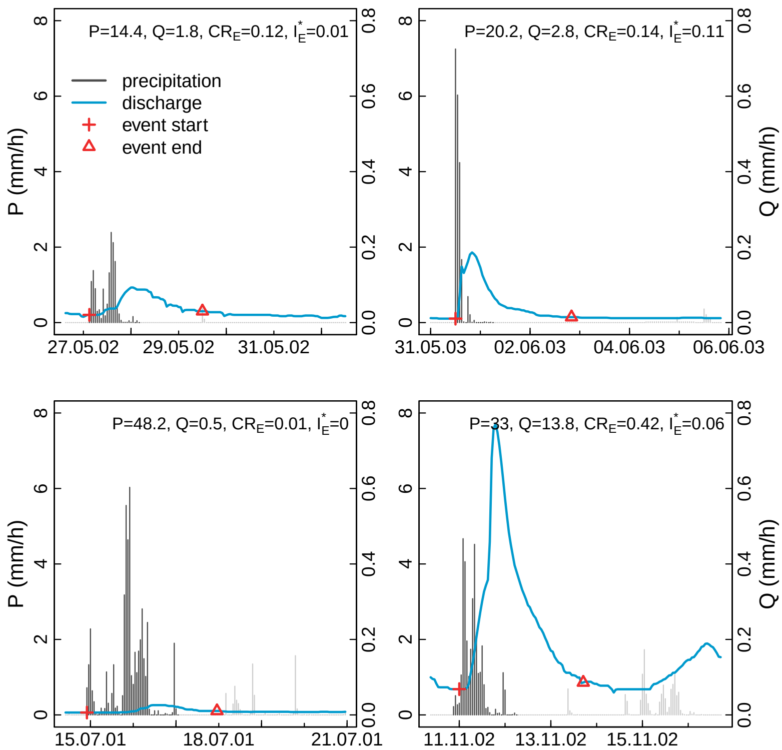

Figure 11. Automated detection of rainfall-runoff events. The plots show results from four selected events from the site TRI3. The examples are selected from different seasonal periods and illustrate different temporal dynamics of forcing and response. The statistics in the top provide event specific totals of rainfall (P) and quickflow (Q), the event runoff coefficient CR_E (Eq. 5) and the normalized temporal intensity change I_E^* (Eq. 7).

Hydrol. Earth Syst. Sci. Discuss., doi:10.5194/hess-2016-109, 2016
Manuscript under review for journal Hydrol. Earth Syst. Sci.
Published: 9 March 2016

Hydrology and Earth System Sciences Discussions
Open Access

Table 1. Physiographic catchment properties in terms of topography, landuse and hydro-meteorology. The columns contain site identifier (ID), catchment size A, mean catchment elevation above sea level (elev), median gradient (ϕ), median gradient times average saturated hyd. conductivity ($\phi \cdot Ks$), relative land coverage ratios for infrastructure (infr), arable land (arab), pasture (past), forest (frst), wetlands (wet) and rock outcrops (rock), the 30 year mean annual precipitation (MAP), four year mean annual precipitation ($\overline{P}$), discharge ($\overline{Q}$), runoff coefficient ($\overline{CR}$), streamflow coefficient of variation (var.c(Q)) and the slope of the flow duration curve between the 33 and 66% percentiles (sFDC). $\overline{CR}$, var.c(Q) and sFDC are dimensionless.

	topography				% land use coverage						hydro-meteorology					
ID	A [km^2]	elev [m]	ϕ [-]	$\phi \cdot Ks$ [m/s]	infr	arab	past	frst	wet	rock	MAP [mm]	$\overline{P}$ [mm]	$\overline{Q}$ [mm]	$\overline{CR}$	var.c(Q)	sFDC
TRI1	88	481	2.8e-02	1.0e-06	0.04	0.54	0.20	0.21	0	0	802	919	0.045	0.43	2.00	-1.46
TRI2	26	460	2.5e-02	9.8e-07	0	0.60	0.12	0.29	0	0	707	801	0.033	0.36	2.20	-1.94
TRI3	93	468	3.8e-02	8.3e-07	0.02	0.62	0.07	0.30	0	0	738	829	0.032	0.33	1.80	-0.99
JUR1	90	518	7.2e-02	2.0e-06	0.01	0.59	0.15	0.26	0	0	833	839	0.046	0.48	0.83	-0.78
BFO1	25	620	6.9e-02	2.5e-06	0	0.35	0.06	0.60	0	0	889	933	0.054	0.51	0.89	-0.61
BFO2	64	635	6.1e-02	1.3e-06	0.02	0.39	0.12	0.47	0.01	0	893	920	0.055	0.53	0.91	-0.64
BFO3	58	624	7.9e-02	1.2e-06	0.01	0.24	0.21	0.55	0	0	908	825	0.052	0.56	1.10	-0.76
MOL1	166	543	1.1e-02	1.6e-08	0.07	0.42	0.29	0.23	0	0	889	973	0.042	0.38	0.83	-0.63
MOL2	163	515	4.0e-02	6.9e-08	0.03	0.28	0.37	0.32	0	0	901	1010	0.045	0.39	0.90	-0.36
MOL3	163	558	1.4e-02	2.0e-08	0.05	0.69	0.10	0.15	0	0	933	1100	0.057	0.45	0.64	-0.27
MOL4	97	517	2.5e-02	3.9e-08	0.04	0.77	0.03	0.15	0	0	888	1016	0.042	0.36	0.93	-0.50
MOL5	133	473	2.0e-02	4.4e-08	0.05	0.81	0.05	0.09	0	0	883	1016	0.047	0.40	1.00	-0.57
MOL6	146	484	4.2e-02	7.8e-08	0.02	0.79	0.04	0.15	0	0	856	721	0.029	0.35	1.60	-0.58
MOL7	87	379	2.4e-02	3.4e-08	0.02	0.73	0.01	0.24	0	0	744	733	0.026	0.31	1.10	-0.71
AFO1	45	840	3.4e-02	3.6e-08	0.01	0.11	0.27	0.62	0	0	1388	1243	0.073	0.51	1.90	-1.32
AFO2	95	777	4.0e-02	9.1e-08	0.01	0.11	0.55	0.31	0.01	0	1292	1466	0.083	0.50	1.30	-0.76
AFO3	136	751	2.2e-02	5.2e-08	0.05	0.12	0.62	0.22	0	0	1198	1015	0.045	0.38	0.72	-0.75
AFO4	12	688	2.9e-02	3.2e-08	0.07	0.32	0.31	0.29	0	0	1114	1024	0.047	0.40	1.20	-1.03
ALP1	47	1279	3.3e-01	1.8e-06	0.00	0.05	0.50	0.45	0	0	2212	2662	0.230	0.75	1.40	-1.14
ALP2	127	1433	4.0e-01	7.7e-07	0.01	0.02	0.55	0.28	0	0.15	2315	2526	0.240	0.83	1.10	-0.83
ALP3	76	1539	5.1e-01	7.6e-07	0.01	0.01	0.59	0.18	0	0.21	2438	2181	0.210	0.86	0.89	-1.07
ALP4	114	1270	4.2e-01	5.1e-07	0.01	0.01	0.25	0.61	0.02	0.09	1826	1684	0.120	0.64	1.00	-0.49

Hydrol. Earth Syst. Sci. Discuss., doi:10.5194/hess-2016-109, 2016
Manuscript under review for journal Hydrol. Earth Syst. Sci.
Published: 9 March 2016

Table 2. Soil properties of the selected headwater catchments: Root zone depth (τ), effective field capacity (eFC_τ), air capacity (AC_τ), field capacity (FC_τ), total pore volume (TPV_τ), and contents of clay, silt, sand and skeleton (skel). FC, eFC, AC and TPV refer to τ. $nsoils$ gives information on the total number of different soils classes within the individual sites. Average saturated hydraulic conductivity (Ks) was estimated based on grain size data Schaap et al. (2001). The soil properties are weighted means (areal share) the national soil map of Germany (BGR, 1995). We also provide aquifer productivity classes (APR) from the international hydrogeological map of Europe (Duscher et al., 2015). The categorical APR values 1, 2, 3 and 4 indicate dominance of highly productive, low to moderately productive conditions, dominance of locally aquiferous rocks and non-aquiferous rocks.

SITE	τ [cm]	eFC_τ [mm]	AC_τ [mm]	FC_τ [mm]	TPV_τ [mm]	clay [%]	silt [%]	sand [%]	skel [%]	Ks [m/s]	n soils	APR
TRI1	68.3	73.9	47.1	262.3	309.4	42.7	9.3	48.6	1.8	3.6e-05	3	2
TRI2	67.1	71.0	49.8	248.4	298.2	39.9	9.0	51.7	1.9	3.9e-05	3	1
TRI3	76.1	94.2	59.2	216.9	276.2	23.3	18.0	58.4	2.5	2.2e-05	4	1/2
JUR1	26.2	32.5	37.0	71.0	108.0	39.2	16.8	43.5	3.7	2.8e-05	6	1
BFO1	60.0	74.0	55.5	110.4	165.9	7.5	9.5	83.2	4.0	3.6e-05	5	4
BFO2	54.8	74.5	40.8	124.0	164.8	12.4	17.0	71.1	3.6	2.1e-05	6	4
BFO3	58.0	67.8	36.4	125.3	161.7	14.3	18.7	67.6	3.8	1.5e-05	5	4
MOL1	85.1	144.8	44.6	330.9	375.5	26.4	58.8	14.4	1.1	1.5e-06	8	1/2/3
MOL2	78.9	146.1	44.3	312.1	356.4	22.3	56.5	21.8	1.4	1.7e-06	4	2
MOL3	86.5	151.3	55.4	290.7	346.1	22.0	48.5	28.9	1.9	1.5e-06	8	2
MOL4	89.2	132.5	46.2	323.9	370.2	22.7	57.2	21.0	1.2	1.6e-06	4	2
MOL5	88.2	138.3	54.3	288.8	343.0	19.0	46.5	34.8	1.9	2.2e-06	12	1/2
MOL6	88.3	129.5	47.7	308.3	355.9	21.0	54.0	24.7	1.3	1.9e-06	3	2
MOL7	90.0	167.1	47.5	328.6	376.1	23.0	66.8	11.2	1.0	1.4e-06	3	2/3
AFO1	100	153.0	76.0	322.5	398.5	21.0	39.0	40.0	2.0	1.1e-06	1	3
AFO2	74.0	149.6	57.0	285.8	342.8	19.8	39.5	40.8	2.2	2.3e-06	5	3
AFO3	79.4	138.4	61.8	266.0	327.8	19.3	33.7	47.1	2.5	2.4e-06	8	3
AFO4	80.0	142.2	59.5	283.4	342.9	20.8	38.0	41.2	1.8	1.1e-06	2	2
ALP1	55.5	90.2	38.5	209.3	247.8	15.8	23.7	60.5	2.5	5.5e-06	2	2/3
ALP2	28.1	42.2	18.8	108.0	126.7	28.2	28.8	44.5	4.2	1.9e-06	5	1/2
ALP3	24.1	35.2	16.0	92.7	108.7	29.4	28.7	42.4	4.4	1.5e-06	5	1/2
ALP4	28.9	41.1	18.7	110.7	129.4	37.5	24.4	39.3	4.3	1.2e-06	5	1

Hydrology and Earth System Sciences
Open Access
Discussions

Table 3. Statistics of the radiation-driven case (baseflow) where the last input in precipitation > 1 mm is at least five days ago: The table contains the sample size (n), Spearmans rank coefficients of correlation (ρ) between the storage measures dS^* and θ^*, between storage measures and normalized specific stream flow depths (Q_b^*) and multiplier and exponent of the fitted non-linear model. As a quality of fit criterion for the latter we provide the root-mean-squared-error normalized by the standard deviation of the sample (nRMSE).

		ρ between			non-linear model		
Site	n	dS^* & θ^*	Q_b^* & dS^*	Q_b^* & θ^*	multiplier	exponent	nRMSE
TRI1	364	*0.2	*0.67	0.01	1.8e-04	1.3	0.56
TRI2	384	-0.01	*0.41	*0.18	1.8e-07	7.2	0.89
TRI3	397	*-0.27	*0.88	-0.02	1.4e-04	1.8	0.44
JUR1	588	0.13	*0.75	-0.01	4.4e-05	2.5	0.70
BFO1	1265	0.09	*0.56	0.06	7.9e-05	2.3	0.65
BFO2	1235	0.02	*0.69	0.03	1.5e-04	1.6	0.68
BFO3	899	*0.30	*0.47	-0.01	3.7e-04	0.8	0.87
MOL1	968	*0.39	*0.84	*0.16	8.1e-03	1.1	0.61
MOL2	654	*-0.24	*0.49	0.10	8.8e-04	2.0	0.84
MOL3	447	-0.02	*0.86	-0.11	5.4e-03	1.6	0.59
MOL4	634	-0.11	*0.50	*0.26	1.7e-03	0.9	0.84
MOL5	1184	*0.18	*0.67	*0.22	2.9e-03	0.7	0.83
MOL6	213	*0.30	*0.84	*0.28	6.0e-03	5.2	0.57
MOL7	1018	*-0.28	*0.16	-0.07	1.1e-03	0.8	1.01
AFO1	250	0.16	*0.45	0.14	5.0e-03	0.3	0.95
AFO2	609	0.04	0.12	*0.54	7.8e-04	15.0	0.92
AFO3	708	*0.21	*0.85	0.07	8.9e-03	2.5	0.49
AFO4	356	0.05	*0.42	*0.22	8.8e-03	0.6	0.86
ALP1	90	NA	NA	NA	NA	NA	NA
ALP2	116	0.03	*0.66	0.19	5.5e-04	2.2	0.64
ALP3	249	0.15	*0.60	0.10	1.0e-08	6.6	0.43
ALP4	80	NA	NA	NA	NA	NA	NA
* cases	-	9	19	7	-	-	-

*-symbols code significant values (p-values<0.001). Note: Snow and frequent rainfall yielded small (n<100) and highly skewed samples in two alpine basins (ALP1 and ALP4). There values are set to NA as a meaningful interpretation is not feasible.

Table 4. Statistics of rainfall-driven conditions: Spearman rank coefficients of correlation (ρ) and Pearsons coefficient of determination (r^2) between the event runoff coeffcients (CR_E) and the three different storage measures (dS^*, θ^* and Q^*), between the storage measures themselves and, results for a multiple linear regression (equation and corresponding r^2) between CR_E and the two most explanatory (uncorrelated) storage measures. If all three storage measures were correlated significantly, both, the equation and the r^2 value were set to NA. We also provide the slope of the linear regression (b) between CR_E and Q^* for cases were the latter were correlated significantly.

		CR_E & dS^*		CR_E & Q^*		CR_E & θ^*		dS^* & θ^*		Q^* & dS^*		Q^* & θ^*		lin reg.	multiple lin. regression	
Site	n	ρ	r^2	ρ	r^2	ρ	r^2	ρ	r^2	ρ	r^2	ρ	r^2	b	equation	r^2
TRI1	51	*0.69	*0.50	*0.81	*0.73	0.38	0.18	0.35	0.11	*0.78	*0.49	0.26	0.18	2.94	*340Q^*+0.087θ^*	0.73
TRI2	40	*0.57	*0.27	*0.82	*0.57	0.44	0.14	0.40	0.11	*0.53	0.24	0.44	*0.30	3.87	*480Q^*-0.086θ^*	0.57
TRI3	37	*0.77	*0.46	*0.88	*0.59	0.39	0.13	0.15	0.01	*0.83	*0.36	0.45	0.26	3.13	*500Q^*-0.069θ^*	0.59
JUR1	40	0.39	0.20	*0.63	*0.29	0.44	0.08	0.41	0.20	*0.63	*0.46	*0.52	*0.43	1.29	NA	NA
BFO1	67	0.30	*0.17	*0.46	*0.16	0.35	0.07	0.37	0.14	0.38	*0.27	*0.54	*0.27	1.09	91Q^*+0.034dS^*	0.22
BFO2	65	*0.51	*0.31	*0.49	*0.24	*0.41	0.09	0.38	0.14	*0.73	*0.46	*0.41	*0.26	1.22	*0.061dS^*+0.057θ^*	0.32
BFO3	52	*0.71	*0.47	*0.67	*0.46	*0.55	*0.25	0.43	0.19	*0.60	*0.43	*0.51	*0.33	1.97	*0.085dS^*+0.14θ^*	0.52
MOL1	66	*0.62	*0.23	*0.67	*0.35	0.32	0.05	0.23	0.04	*0.85	*0.63	0.29	0.03	2.68	*490Q^*+0.13θ^*	0.37
MOL2	67	0.26	0.07	*0.52	*0.19	0.18	0.03	0.11	0	*0.52	*0.24	*0.47	*0.24	1.86	NA	NA
MOL3	73	*0.49	*0.22	*0.49	*0.20	0.34	0.06	0.19	0.01	*0.73	*0.46	0.38	*0.17	1.47	*0.097dS^*+0.14θ^*	0.26
MOL4	70	0.18	0.07	*0.56	*0.20	*0.55	*0.18	0.19	0.06	*0.61	*0.32	*0.49	*0.29	1.90	NA	NA
MOL5	77	*0.55	*0.30	*0.72	*0.29	*0.56	*0.24	*0.56	*0.21	*0.74	*0.46	*0.56	*0.31	1.60	NA	NA
MOL6	40	0.42	0.20	0.49	0.24	0.30	0.08	0.25	0.04	*0.51	0.15	*0.61	*0.48	NA	NA	NA
MOL7	38	0.30	0.16	0.48	0.26	0.50	*0.28	0.15	0.01	-0.08	0	0.36	0.22	NA	0.42θ^*+300Q^*	0.37
AFO1	54	0.01	0	*0.64	*0.27	*0.57	*0.26	0.23	0.04	-0.05	0.01	*0.58	*0.53	1.65	*380Q^*-0.059dS^*	0.28
AFO2	61	0.19	0.04	*0.48	0.07	0.33	0.07	0.29	0.03	0.25	0.06	0.39	*0.24	0.75	100Q^*+0.26θ^*	0.09
AFO3	38	0.51	*0.31	0.45	0.24	0.16	0.03	0.15	0	*0.89	*0.69	0.17	0.02	NA	*0.11dS^*+0.085θ^*	0.33
AFO4	65	*0.55	*0.25	*0.58	*0.20	*0.45	0.11	0.30	0.06	*0.55	*0.30	*0.41	*0.21	1.41	NA	NA
ALP1	78	0.32	0.09	0.30	0.09	*0.38	0.12	0.34	*0.18	0.22	0.09	*0.42	*0.40	NA	0.14θ^*+0.034dS^*	0.15
ALP2	39	0.30	0.15	0.42	0.20	0.39	0.17	0.13	0.01	0.29	0.13	*0.57	*0.28	NA	31Q^*+0.04dS^*	0.26
ALP3	30	0.52	0.22	0.01	0.06	0.41	*0.34	0.30	0.13	0.24	0.14	0.41	0.19	NA	0.016dS^*+0.18θ^*	0.42
ALP4	26	0.13	0	0.23	0.15	*0.72	*0.50	0.33	0.12	0.07	0.03	0.29	0.28	NA	*0.24θ^*+1.8Q^*	0.5
* count	-	9	11	15	14	8	7	1	2	14	13	12	15	-	-	

*-symbols code significant ρ and r^2 values (p-value<0.001) and significant regressors in the case of the multiple lin. regression.

Table 5. Mean seasonal winter (CR_W), summer (CR_S) and annual runoff coefficients (CR_{yr}) as indicated by the slope of regression lines fitted to the normalized double mass curves. CE_{yr} represents the mean annual evapotranspiration ratio. The inter-annual variations of these quantities within the hydrological years ('99-'03) is quantified using the mean absolute deviation which we provide by mad_{CR_W}, mad_{CR_S}, $mad_{CR_{YR}}$ and $mad_{CE_{YR}}$, respectively. All quantities are dimensionless.

Site	CR_W	CR_S	CR_{yr}	CE_{yr}	mad_{CR_W}	mad_{CR_S}	$mad_{CR_{YR}}$	mad_{CE_W}
TRI1	0.72	0.12	0.43	0.53	0.058	0.030	0.031	0.018
TRI2	0.70	0.07	0.37	0.68	0.198	0.027	0.105	0.021
TRI3	0.55	0.12	0.34	0.63	0.133	0.024	0.069	0.022
JUR1	0.73	0.25	0.48	0.56	0.150	0.017	0.054	0.015
BFO1	0.82	0.28	0.52	0.48	0.169	0.037	0.068	0.033
BFO2	0.85	0.30	0.54	0.47	0.143	0.020	0.067	0.029
BFO3	0.93	0.29	0.57	0.51	0.173	0.034	0.089	0.024
MOL1	0.60	0.24	0.38	0.62	0.103	0.040	0.021	0.023
MOL2	0.56	0.27	0.40	0.58	0.080	0.022	0.049	0.042
MOL3	0.62	0.34	0.46	0.57	0.069	0.019	0.045	0.035
MOL4	0.56	0.23	0.37	0.61	0.084	0.021	0.051	0.048
MOL5	0.69	0.22	0.41	0.58	0.055	0.028	0.026	0.023
MOL6	0.60	0.20	0.36	0.66	0.066	0.018	0.025	0.015
MOL7	0.35	0.27	0.31	0.68	0.139	0.089	0.031	0.052
AFO1	0.72	0.35	0.51	0.46	0.031	0.120	0.042	0.053
AFO2	0.68	0.34	0.49	0.48	0.036	0.099	0.043	0.052
AFO3	0.56	0.24	0.38	0.62	0.130	0.068	0.031	0.056
AFO4	0.66	0.22	0.39	0.64	0.050	0.090	0.030	0.092
ALP1	0.89	0.50	0.75	0.24	0.098	0.088	0.031	0.031
ALP2	0.71	0.82	0.83	0.17	0.067	0.161	0.047	0.015
ALP3	0.64	0.84	0.86	0.18	0.082	0.109	0.025	0.017
ALP4	0.66	0.53	0.64	0.33	0.064	0.066	0.032	0.051
mean	0.67	0.32	0.49	0.51	0.10	0.06	0.046	0.035

Hydrol. Earth Syst. Sci. Discuss., doi:10.5194/hess-2016-109, 2016
Manuscript under review for journal Hydrol. Earth Syst. Sci.
Published: 9 March 2016

Table 6. Link table that relates the site identifiers (ID) introduced in section 3 to the corresponding gauge and stream names. Gauge locations are provided in Gauß-Krüger zone 4 coordinates (GKR and GKH).

ID	Gauge	Stream	GKR	GKH
TRI1	Reichenbach (REIB)	Wörnitz	4373327	5449863
TRI2	Binzwangen (BINZ)	Altmühl	4381996	5473002
TRI3	Bechhofen (BECH)	Wieseth	4394270	5447640
JUR1	Holnstein (HOLN)	Unterbürger Laber	4464800	5442860
BFO1	Gartenried (GART)	Murach	4532661	5483477
BFO2	Untereppenried (UEPR)	Ascha	4533425	5477338
BFO3	Tiefenbach (TIEF)	Bayerische Schwarzach	4543360	5477800
MOL1	Roth (ROTR)	Roth	4363140	5360723
MOL2	Fleinhausen (FLEI)	Zusam	4394141	5358887
MOL3	Mering (MERI)	Paar	4424840	5348870
MOL4	Odelzhausen (ODZH)	Glonn	4440860	5353360
MOL5	Appolding (APPO)	Strogen	4498575	5364071
MOL6	Dietelskirchen (DIKI)	Kleine Vils	4525540	5373175
MOL7	Wallersdorf (WALR)	Reißingerbach	4554850	5400160
AFO1	Unterthingau (alt) (UTHI)	Kirnach	4388313	5294058
AFO2	Hörmanshofen (HOER)	Geltnach	4399272	5299593
AFO3	Buchloe (BUCH)	Gennach	4404574	5323974
AFO4	Herrsching (HERR)	Kienbach	4438860	5318140
ALP1	Gunzesried (GZRI)	Gunzesrieder Ach	4366798	5266382
ALP2	Reckenberg (RECK)	Ostrach	4373822	5264305
ALP3	Oberstdorf (OBTR)	Trettach	4370128	5255320
ALP4	Oberammergau (OAMM)	Ammer	4429723	5273332